UNIVERSITÀ DI SIENA 1240

USiena

Genome-wide association study identifies five new susceptibility loci for primary angle closure glaucoma

This is the peer reviewed version of the following article:

Original:

Khor, C.C., Do, T., Jia, H., Nakano, M., George, R., Abu Amero, K., et al. (2016). Genome-wide association study identifies five new susceptibility loci for primary angle closure glaucoma. NATURE GENETICS, 48(5), 556-562 [10.1038/ng.3540].

Availability:

This version is availablehttp://hdl.handle.net/11365/999469 since 2016-11-20T17:33:13Z

Published:

DOI:10.1038/ng.3540

Terms of use:

Open Access

The terms and conditions for the reuse of this version of the manuscript are specified in the publishing policy. Works made available under a Creative Commons license can be used according to the terms and conditions of said license.
For all terms of use and more information see the publisher's website.

(Article begins on next page)

17 April 2024

Nature Genetics 2016

Genome-wide association study identifies five new susceptibility loci for primary angle closure glaucoma

Chiea chuen khor[1–3,124], Tan do[4,124], Hongyan Jia[5,124], masakazu nakano[6,124], Ronnie george[7,124], khaled Abu-Amero[8,9,124], Roopam duvesh[10,124], li Jia chen[11,124], Zheng li[1], monisha e nongpiur[2], shamira A Perera[2], chunyan Qiao[5], Hon-tym wong[12], Hiroshi sakai[13], mônica Barbosa de melo[14], mei-chin lee[2], Anita s chan[2], Yaakub Azhany[15], thi lam Huong dao[4], Yoko Ikeda[16], Rodolfo A Perez-grossmann[17], Tomasz Zarnowski[18], Alexander c day[19–21], Jost B Jonas[22], Pancy o s tam[11], tuan Anh tran[23], Humaira Ayub[24], Farah Akhtar[25], shazia micheal[26], Paul t k chew[27], leyla A Aljasim[28], tanuj dada[29], tam thi luu[30], mona s Awadalla[31], naris kitnarong[32], Boonsong wanichwecharungruang[33,34], Yee Yee Aung[35], Jelinar mohamed-noor[36], saravanan Vijayan[10], sripriya sarangapani[37], Rahat Husain[2,38], Aliza Jap[2,38], mani Baskaran[2], david goh[2], daniel H su[2], Huaizhou wang[5], Vernon k Yong[12], leonard w Yip[12], tuyet Bach trinh[23], manchima makornwattana[39], thanh thu nguyen[40], edgar U leuenberger[41,42], ki-Ho Park[43], widya Artini wiyogo[44,45], Rajesh s kumar[46], celso tello[47], Yasuo kurimoto[48], suman s thapa[49], kessara Pathanapitoon[50], John F salmon[51], Yong Ho sohn[52], Antonio Fea[53], mineo ozaki[54,55], Jimmy s m lai[56], Visanee tantisevi[57], chaw chaw khaing[58], takanori mizoguchi[59], satoko nakano[60], chan-Yun kim[61], guangxian tang[62], sujie Fan[63], Renyi wu[64], Hailin meng[65], thi thuy giang nguyen[4], tien dat tran[4], morio Ueno[16], Jose maria martinez[66], norlina Ramli[67,68], Yin mon Aung[69,70], Rigo daniel Reyes[71,72], Stephen A Vernon[73,74], Seng kheong Fang[75], Zhicheng Xie[1], Xiao Yin chen[1], Jia nee Foo[1], kar seng sim[1], Tina t wong[2], desmond t Quek[2], Rengaraj Venkatesh[76], srinivasan kavitha[76], subbiah R krishnadas[77], nagaswamy soumittra[37], Balekudaru shantha[7], Boon-Ang lim[12], Jeanne ogle[12], José P c de Vasconcellos[78], Vital P costa[77], Ricardo Y Abe[77], Bruno B de souza[14], chelvin c sng[27], maria c Aquino[27], ewa kosior-Jarecka[18], guillermo Barreto Fong[79], Vania castro tamanaja[80], Ricardo Fujita[81], Yuzhen Jiang[19–21], naushin waseem[19,21], sancy low[19–21], Huan nguyen Pham[23], sami Al-shahwan[28], e Randy craven[28,82], muhammad Imran khan[83], Rrima dada[29], kuldeep mohanty[29], muneeb A Faiq[29], Alex w Hewitt[84,85], kathryn P Burdon[31,84], eng Hui gan[36], Anuwat Prutthipongsit[39], thipnapa Patthanathamrongkasem[39], mary Ann t catacutan[41], Irene R Felarca[41], chona s liao[41], emma Rusmayani[44], Vira wardhana Istiantoro[44], giulia consolandi[53], giulia Pignata[53], carlo lavia[53], Prin Rojanapongpun[57], lerprat mangkornkanokpong[86], sunee chansangpetch[86], Jonathan c H chan[87], Bonnie n k choy[56], Jennifer w H shum[56], Hlaing may than[88], khin thida oo[69,70], Aye thi Han[69,70], Victor H Yong[2], Xiao-Yu ng[2], shuang Ru goh[2], Yaan Fun chong[2], martin l Hibberd[1], mark seielstad[89], eileen Png[1], sarah J dunstan[90,91], nguyen Van Vinh chau[92], Jinxin Bei[93,94], Yi Xin Zeng[93–95], Abhilasha karkey[96], Buddha Basnyat[96], Francesca Pasutto[97], daniela Paoli[98], Paolo Frezzotti[99], Jie Jin wang[100], Paul mitchell[100], John H Fingert[101,102], R Rand Allingham[2,103], michael A Hauser[2,103,104], soon thye lim[105], soo Hong chew[106], Richard P ebstein[107], Anavaj sakuntabhai[108,109], kyu Hyung Park[110], Jeeyun Ahn[111], greet Boland[112], Harm snippe[112], Richard stead[73], Raquel Quino[71], su nyunt Zaw[69,70], Urszula lukasik[18], Rohit shetty[46], mimiwati Zahari[67,68], Hyoung won Bae[61], nay lin oo[58], toshiaki kubota[60], Anita manassakorn[57], wing lau Ho[86], laura dallorto[53], Young Hoon Hwang[52], christine A kiire[51], masako kuroda[48], Zeiras eka djamal[44], Jovell Ian m Peregrino[41], Arkasubhra ghosh[46,113], Jin wook Jeoung[43], tung s Hoan[40], nuttamon srisamran[39], thayanithi sandragasu[36], saw Htoo set[35], Vi Huyen doan[30], shomi s Bhattacharya[21], ching-lin Ho[2], donald t tan[2], Ramanjit sihota[29], seng-chee loon[27], kazuhiko mori[16], shigeru kinoshita[16], Anneke I den Hollander[26,83], Raheel Qamar[24,114], Ya-Xing wang[115], Yik Y teo[1,116–119], e-shyong tai[116,120], curt Hartleben-matkin[121], david lozano-giral[122], seang mei saw[2,116], ching-Yu cheng[2,27], Juan c Zenteno[122,123], chi Pui Pang[11], Huong t t Bui[23], owen Hee[12], Jamie e craig[31], deepak P edward[28,82], michiko Yonahara[13], Jamil miguel neto[78], maria l guevara-Fujita[81], liang Xu[115], Robert Ritch[47], Ahmad tajudin liza-sharmini[15], tien Y wong[2], saleh Al-obeidan[8], nhu Hon do[4,125], Periasamy sundaresan[10,125], clement c tham[11,125], Paul J Foster[19–21,125], lingam Vijaya[2,7,125], kei tashiro[6,125], eranga n Vithana[2,125], ningli wang[5,115,125] & tin Aung[2,27,125]

[1]Genome Institute of Singapore, A-STAR, Singapore. [2]Singapore Eye Research Institute, Singapore National Eye Centre and Eye ACP, Duke–National University of Singapore, Singapore. [3]Department of Biochemistry, National University of Singapore, Singapore. [4]Vietnam National Institute of Ophthalmology, Hanoi, Vietnam. [5]Beijing Tongren Eye Center, Beijing Tongren Hospital, Capital Medical University, Beijing Ophthalmology and Visual Science Key Laboratory, Beijing, China. [6]Department of Genomic Medical Sciences, Kyoto Prefectural University of Medicine, Kyoto, Japan. [7]Jadhavbhai Nathamal Singhvi Department of

Glaucoma, Medical Research Foundation, Sankara Nethralaya, Chennai, India. [8]Department of Ophthalmology, College of Medicine, King Saud University, Riyadh, Saudi Arabia. [9]Department of Ophthalmology, College of Medicine, University of Florida, Jacksonville, Florida, USA. [10]Department of Genetics, Aravind Medical Research Foundation, Madurai, India. [11]Department of Ophthalmology and Visual Sciences, Chinese University of Hong Kong, Hong Kong, China. [12]Department of Ophthalmology, Tan Tock Seng Hospital, NHG Eye Institute, Singapore. [13]Department of Ophthalmology, University of the Ryukyus, Okinawa, Nishihara, Japan. [14]Center of Molecular Biology and Genetic Engineering, University of Campinas, Campinas, Brazil. [15]Department of Ophthalmology, School of Medical Sciences, Health Campus, Universiti Sains Malaysia and Hospital Universiti Sains Malaysia, Kelantan, Malaysia. [16]Department of Ophthalmology, Kyoto Prefectural University of Medicine, Kyoto, Japan. [17]Instituto de Glaucoma y Catarata, Lima, Peru. [18]Department of Diagnostics and Microsurgery of Glaucoma, Medical University, Lublin, Poland. [19]NIHR Biomedical Research Centre for Ophthalmology at Moorfields Eye Hospital and University College London Institute of Ophthalmology, London, UK. [20]Glaucoma Service, Moorfields Eye Hospital NHS Foundation Trust, London, UK. [21]Division of Genetics, UCL Institute of Ophthalmology, London, UK. [22]Department of Ophthalmology, Medical Faculty Mannheim of the Ruprecht Karls University Heidelberg, Heidelberg, Germany. [23]Ho Chi Minh City Eye Hospital, Ho Chi Minh City, Vietnam. [24]Department of Biosciences, COMSATS Institute of Information Technology, Islamabad, Pakistan. [25]Pakistan Institute of Ophthalmology, Al-Shifa Trust Eye Hospital, Rawalpindi, Pakistan. [26]Department of Ophthalmology, Radboud University Medical Centre, Nijmegen, the Netherlands. [27]Department of Ophthalmology, National University Health System, Yong Loo Lin School of Medicine, National University of Singapore, Singapore. [28]King Khaled Eye Specialist Hospital, Riyadh, Saudi Arabia. [29]All India Institute of Medical Sciences, New Delhi, India. [30]Department of Glaucoma, Da Nang Eye Hospital, Da Nang City, Vietnam. [31]Department of Ophthalmology, Flinders University, Flinders Medical Centre, Adelaide, South Australia, Australia. 32Department of Ophthalmology, Faculty of Medicine Siriraj Hospital, Mahidol University, Bangkok, Thailand. 33Glaucoma Services, Department of Ophthalmology, Rajavithi Hospital, Bangkok, Thailand. 34College of Medicine, Rangsit University, Bangkok, Thailand. 35Mandalay Eye Department, Mandalay Eye ENT Hospital, University of Medicine Mandalay, Mandalay, Myanmar. 36Department of Ophthalmology, Hospital Kuala Lumpur, Kuala Lumpur, Malaysia. 37Vision Research Foundation, Sankara Nethralaya, Chennai, India, 38Division of Ophthalmology, Changi General Hospital, Singapore. 39Department of Ophthalmology, Thammasat University Faculty of Medicine, Rangsit, Thailand. 40Eye Department, Viet Tiep General Hospital, Hai Phong, Vietnam. 41Asian Eye Institute, Manila, Philippines. 42Division of Ophthalmology, University of the East, Manila, Philippines. 43Department of Ophthalmology, Seoul National University College of Medicine, Seoul, Republic of Korea. 44Glaucoma Service Jakarta Eye Center, Jakarta, Indonesia. 45Faculty of Medicine, University of Indonesia, Jakarta, Indonesia. 46Narayana Nethralaya Eye Hospital, Bangalore, India. 47Einhorn Clinical Research Center, New York Eye and Ear Infirmary of Mount Sinai, New York, New York, USA. 48Department of Ophthalmology, Kobe City Medical Center General Hospital, Kobe, Japan. 49Nepal Glaucoma Eye Clinic, Tilganga Institute of Ophthalmology, Kathmandu, Nepal. 50Department of Ophthalmology, Faculty of Medicine, Chiang Mai University, Chiang Mai, Thailand. 51Oxford Eye Hospital, John Radcliffe Hospital, Oxford University Hospitals NHS Trust, Oxford, UK. 52Department of Ophthalmology, Konyang University, Kim's Eye Hospital, Myung-Gok Eye Research Institute, Seoul, Republic of Korea. 53Dipartimento di Scienze Chirurgiche, Università di Torino, Turin, Italy. 54Ozaki Eye Hospital, Hyuga, Japan. 55Department of Ophthalmology, Faculty of Medicine, University of Miyazaki, Miyazaki, Japan. 56Department of Ophthalmology, University of Hong Kong, Hong Kong, China. 57Department of Ophthalmology, Faculty of Medicine, Chulalongkorn University, Bangkok, Thailand. 58Department of Ophthalmology, No. 1 Defence Services General Hospital, Yangon, Myanmar. 59Mizoguchi Eye Hospital, Sasebo, Japan. 60Department of Ophthalmology, Oita University Faculty of Medicine, Oita, Japan. 61Department of Ophthalmology, Yonsei University College of Medicine, Seoul, Republic of Korea. 62Shijiazhuang First Eye Hospital, Shijiazhuang, China. 63Handan Eye Hospital, Handan, China. 64Eye Institute and Affiliated Xiamen Eye Center, Xiamen University, Fujian Provincial Key Laboratory of Ophthalmology and Visual Science, Xiamen, China. 65Anyang Eye Hospital, Anyang, China. 66Department of Ophthalmology, Pasig City General Hospital, Pasig City, Philippines. 67University of Malaya, Eye Research Centre, Kuala Lumpur, Malaysia. 68Department of Ophthalmology, Faculty of Medicine, University of Malaya, Kuala Lumpur, Malaysia. 69Myanmar Eye Centre, Pun Hlaing Silom Hospital, Yangon, Myanmar. 70Myanmar Eye Centre, Shwe La Min Hospital, Yangon, Myanmar. 71Department of Ophthalmology/Glaucoma Section, Asian Hospital and Medical Center, Muntinlupa City, Philippines. 72Binan Doctors Eye Center, Binan Doctors Hospital, Laguna, Philippines. 73Department of Ophthalmology, University Hospital Nottingham, University of Nottingham, Nottingham, UK. 74BMI Park Hospital Nottingham, Nottingham, UK. 75International Specialist Eye Centre, Kuala Lumpur, Malaysia. 76Glaucoma Clinic, Aravind Eye Hospital, Pondicherry, India. 77Glaucoma Clinic, Aravind Eye Hospital, Madurai, India. 78Department of Ophthalmology, Faculty of Medical Sciences, University of Campinas, Campinas, Brazil. 79Instituto de Ciencias Médicas, Lima, Peru. 80Hospital Nacional Arzobispo Loayza, Lima, Peru. 81Centro de Genética y Biología Molecular, Universidad de San Martín de Porres, Lima, Peru. 82Wilmer Eye Institute, Johns Hopkins Hospital School of Medicine, Baltimore, Maryland, USA. 83Department of Human Genetics, Radboud University Medical Centre, Nijmegen, the Netherlands. 84Menzies Institute for Medical Research, University of Tasmania, Hobart, Tasmania, Australia. 85Centre for Eye Research Australia, University of Melbourne, Royal Victorian Eye and Ear Hospital, Melbourne, Victoria, Australia. 86Department of Ophthalmology, King Chulalongkorn Memorial Hospital, Bangkok, Thailand. 87Department of Ophthalmology, Queen Mary Hospital, Hong Kong, China. 88Department of Ophthalmology, North Okkalarpa General Hospital, Yangon, Myanmar. 89Institute for Human Genetics, University of California, San Francisco, San Francisco, California, USA. 90Oxford University Clinical Research Unit, Ho Chi Minh City, Vietnam. 91Peter Doherty Institute for Infection and Immunity, University of Melbourne, Melbourne, Victoria, Australia. 92Hospital for Tropical

Diseases, Ho Chi Minh City, Vietnam. 93Sun Yat-Sen University Cancer Center, State Key Laboratory of Oncology in South China, Collaborative Innovation Center for Cancer Medicine, Guangzhou, China. 94Department of Experimental Research, Sun Yat-sen University Cancer Center, Guangzhou, China. 95Peking Union Medical College, Beijing, China. 96Oxford University Clinical Research Unit–Nepal, Patan Academy of Health Sciences, Patan Hospital, Patan, Nepal. 97Institute of Human Genetics, Friedrich Alexander Universität Erlangen-Nürnberg (FAU), Erlangen, Germany. 98Department of Ophthalmology, Monfalcone Hospital, Gorizia, Italy. 99Department of Surgery, Section of Ophthalmology, University of Siena, Siena, Italy. 100Centre for Vision Research, Department of Ophthalmology, Westmead Institute for Medical Research, University of Sydney, Sydney, New South Wales, Australia. 101Department of Ophthalmology and Visual Sciences, Carver College of Medicine, University of Iowa, Iowa City, Iowa, USA. 102Wynn Institute for Vision Research, University of Iowa, Iowa City, Iowa, USA. 103Department of Ophthalmology, Duke University Eye Center, Durham, North Carolina, USA. 104Department of Medicine, Duke University Medical Center, Durham, North Carolina, USA. 105Division of Medical Oncology, National Cancer Centre, Singapore. 106Department of Economics, National University of Singapore, Singapore. 107Department of Psychology, National University of Singapore, Singapore. 108Institut Pasteur, Functional Genetics of Infectious Diseases Unit, Department of Genomes and Genetics, Paris, France. 109Centre National de la Recherche Scientifique, Unité de Recherche Associée 3012, Paris, France. 110Department of Ophthalmology, Seoul National University Bundang Hospital, Gyeonggi, Republic of Korea. 111Department of Ophthalmology, Seoul Metropolitan Government Seoul National University Boramae Medical Center, Seoul, Republic of Korea. 112Department of Medical Microbiology and Virology, University Medical Center Utrecht, Utrecht, the Netherlands. 113GROW Research Laboratory, Narayana Nethralaya Foundation, Bangalore, India. 114Department of Biochemistry, Al-Nafees Medical College and Hospital, Isra University, Islamabad, Pakistan. 115Beijing Institute of Ophthalmology, Beijing Tongren Hospital, Capital Medical University, Beijing, China. 116Saw Swee Hock School of Public Health, National University of Singapore, Singapore. 117Life Sciences Institute, National University of Singapore, Singapore. 118National University of Singapore Graduate School for Integrative Science and Engineering, National University of Singapore, Singapore. 119Department of Statistics and Applied Probability, National University of Singapore, Singapore. 120Department of Medicine, Yong Loo Lin School of Medicine, National University of Singapore, Singapore. 121Department of Glaucoma, Institute of Ophthalmology 'Conde de Valenciana', Mexico City, Mexico. 122Department of Genetics, Institute of Ophthalmology 'Conde de Valenciana', Mexico City, Mexico. 123Department of Biochemistry, Faculty of Medicine, Universidad Nacional Autónoma de México, Mexico City, Mexico. 124These authors contributed equally to this work. 125

Correspondence should be addressed to C.C. Khor (khorcc@gis.a-star.edu.sg), N. Wang (wningli@vip.163.com) or T.A. (aung_tin@yahoo.co.uk).

Abstract

Primary angle closure glaucoma (PACG) is a major cause of blindness worldwide. We conducted a genome-wide association study (GWAS) followed by replication in a combined total of 10,503 PACG cases and 29,567 controls drawn from 24 countries across Asia, Australia, Europe, North America, and South America. We observed significant evidence of disease association at five new genetic loci upon meta-analysis of all patient collections. These loci are at EPDR1 rs3816415 (odds ratio (OR) = 1.24, P = 5.94 × 10−15), CHAT rs1258267 (OR = 1.22, P = 2.85 × 10−16), GLIS3 rs736893 (OR = 1.18, P = 1.43 × 10−14), FERMT2 rs7494379 (OR = 1.14, P = 3.43 × 10−11), and DPM2–FAM102A rs3739821 (OR = 1.15, P = 8.32 × 10−12). We also confirmed significant association at three previously described loci (P < 5 × 10−8 for each sentinel SNP at PLEKHA7, COL11A1, and PCMTD1–ST18)1, providing new insights into the biology of PACG.

Main

Glaucoma is the most common cause of irreversible blindness worldwide2. The main forms of glaucoma are primary open angle glaucoma (POAG), PACG, and exfoliation glaucoma. All three forms of glaucoma show familial clustering, suggesting a substantial genetic component in pathogenesis. Recent genetic studies have implicated several distinct loci associated with each of these types of glaucoma[1,3,4,5,6]. For PACG, the epidemiological risk factors include advancing age, female sex, and East Asian ancestry[7,8]. Up to 80% of the estimated 15 million people afflicted with PACG live in Asia[9], where the disease is responsible for a high proportion of blindness[10,11,12,13]. Patients either present with acute primary angle closure (APAC) or have PACG upon presentation (Supplementary Note). We previously performed a GWAS of PACG susceptibility on 1,854 PACG cases and 9,608 controls with replication in 1,917 cases and 8,943 controls, identifying three susceptibility loci1.

We now expand the study to perform a discovery-stage GWAS on a combined total of 6,525 PACG cases and 19,929 controls, which were enrolled from 15 countries spanning East Asia, South Asia, Europe, and South America (Fig. 1 and Supplementary Table 1). We applied routine quality control checks for SNPs and samples as is usually done for GWAS analyses (Online Methods). SNPs at ten distinct loci surpassed $P < 1 \times 10^{-6}$ (Supplementary Table 2), a threshold we took to be indicative of suggestive evidence of association with disease14. Three of these loci have previously been reported (Fig. 2 and Supplementary Table 3)[1]. We then subjected the ten sentinel SNPs representing each of the ten independent loci to replication genotyping in a further 3,978 cases and 9,638 controls from 14 countries (Supplementary Table 1). Significant replication was observed at eight distinct loci (Table 1 and Supplementary Table 2; the initial associations observed at FNDC3B rs16856870 on chromosome 3 and SLC38A6 rs10483730 on chromosome 14 did not replicate), and meta-analysis of all discovery and replication samples totaling 10,503 PACG cases and 29,567 controls showed genome-wide significant evidence of association for the eight loci with PACG (Fig. 2 and Table 1). This two-stage study design is powered to detect effect sizes as low as 1.15 with minor allele frequencies (MAFs) as low as 0.15 at genome-wide significance (Supplementary Table 4).

We next asked whether heterogeneity in genetic effect sizes exists across ancestry groups and geographical locations and found that only EPDR1 rs3816415 showed discernable evidence of heterogeneity in the overall meta-analysis (Phet = 0.0072, I2 index = 43.0%). Closer scrutiny showed that effect sizes were consistently larger in Europeans (OR = 1.42) than in Asians (OR = 1.21) (Fig. 3 and Table 1), despite similar risk allele frequencies across the ancestry groups (Supplementary Table 5). This discrepancy could be due either to more unreliable estimation in Europeans because of the smaller sample size in comparison to Asians (n = 1,105 European PACG cases versus 9,398 Asian PACG cases) or to a genuine difference in effect between Asians and Europeans[15,16,17]. We did not observe significant heterogeneity in effect sizes at the other four loci (Fig. 3 and Table 1). Imputation-based fine-mapping and regional association analysis showed that each SNP locus mapped distinctly among its nearest genes, mostly framed by recombination events (Supplementary Fig. 1). However, as the GWAS approach assays mostly common, representative genetic variants across the human genome, we are unable to exclude the possibility that the identified SNPs at each locus could be tagging functional variants that are exerting control on distant gene targets in a position- and orientation-independent manner[18,19].

We next examined the ocular expression of genes located in the newly identified PACG loci by RT–PCR. We detected mRNA expression of *EPDR1*, *GLIS3*, *FERMT2*, *DPM2*, *PIP5KL1*, and *FAM102A* in human ocular anterior segment tissues such as the iris, ciliary body, and trabecular meshwork (Supplementary Fig. 2a). We also observed mRNA expression of all six genes in the cornea, lens, retina, choroid, optic nerve head, and optic nerve. We also investigated the distribution of the encoded proteins of these genes in ocular tissues by immunohistochemical labeling of sections of a normal human eye (Supplementary Figs. 3,4,5,6,7,8,9), testing for tissue specificity of expression through immunoblot analysis in ocular-tissue-derived cell lines (Supplementary Fig. 2b–h). Overall, protein expression and localization corroborated the mRNA data, except in the case of GLIS3, where pronounced protein expression was seen in the iris, different to what was observed in mRNA expression analysis (Supplementary Fig. 2a). This difference may be attributed to the insensitivity of the RT–PCR technique for transcripts present at low levels.

EPDR1 encodes a glycosylated type II transmembrane protein known as ependymin-related 1. It potentially has a role in cell adhesion, as it is similar to protocadherins and ependymins[20]. SNP *EPDR1* rs16879765 has been shown to be significantly associated with Dupuytren's contracture, an inherited disorder of connective tissues[21]. Our genome-wide significant association at *EPDR1* for PACG is marked by the sentinel SNP rs3816415, which is very poorly correlated with rs16879765 despite being located less than 1 kb away. This pleiotropic association with *EPDR1* merits further study and highlights the relevance of cell adhesion molecules more broadly in PACG pathology.

SNP rs3739821 is located in an intergenic region between *DPM2* and *FAM102A*, a gene yet to be fully characterized. Mutations in *DPM2* have been linked to congenital defects in glycosylation[22], leading to severe

neurological phenotypes. Although not much is known about *FAM102A* except that its expression is sensitive to the addition of β-estradiol[23], the nearby *PIP5KL1* gene (Supplementary Fig. 1) has been reported to be involved in cell proliferation[24] and potentially in tumorigenesis. Our expression analysis showed that all three genes (*FAM102A*, *DPM2*, and *PIP5KL1*) were expressed in all eye tissues tested, thus providing biological support for their involvement in PACG (Supplementary Figs. 2 and 7,8,9). Further fine-mapping work is needed to identify the causative gene in this locus.

CHAT on chromosome 10 encodes choline acetyltransferase. This is an enzyme responsible for synthesis of the neurotransmitter acetylcholine, which has a role in pupillary constriction. Anticholinergic medications can precipitate acute PACG via pupillary dilatation and subsequent pupillary block[25,26]. Therefore, it is plausible that natural genetic variation in a gene influencing acetylcholine metabolism could influence risk for PACG.

FERMT2 encodes a protein called pleckstrin-homology-domain-containing family C member 1 (PLEKHC1), a component of the extracellular matrix, and could thus have a role in cell adhesion[27]. PLEKHC1 belongs to the same pleckstrin family of proteins as PLEKHA7, and we previously showed that common SNPs mapping to *PLEKHA7* are significantly associated with susceptibility to PACG[1]. Our current observation of genome-wide significant associations at *FERMT2* and *EPDR1*, as well as the previous report of *PLEKHA7*, strongly implicates the cell–cell adhesion process as being important in the pathogenesis of PACG.

GLIS3 is a member of the GLI-similar subfamily of Krüppel-like zinc-finger proteins[28]. Earlier studies have shown that mutations in *GLIS3* cause neonatal diabetes and congenital hypothyroidism[29]. SNP markers mapping close to *GLIS3* have been observed to be significantly associated with type 1 diabetes in Europeans (rs7020673)[30], type 2 diabetes in East Asians (rs7041847)[31], and fasting plasma glucose levels in a large meta-analysis of European collections (rs7034200)[32]. These SNPs are independent from rs736893, which we observe here to be associated with PACG. These observations implicate yet unknown metabolic pathways that could contribute to PACG pathogenesis.

We next looked up reported loci showing genome-wide significant association with POAG[3,4,33,34] in our PACG discovery GWAS data set, as susceptibility variants for the two common forms of glaucoma could potentially be shared. We observed evidence of association at *ARHGEF12* rs2276035 and *GAS7* rs12150284. For both loci, the direction of effect was consistent in PACG and POAG (Supplementary Table 6). Reciprocally, we also assessed all eight genome-wide significant PACG loci in 968 POAG cases and 3,916 controls of Singaporean Chinese descent[35] but did not observe consistent evidence of association between the PACG loci and POAG (Supplementary Table 7).

Both ocular axial length and anterior chamber depth have previously been reported as anatomical risk factors for PACG, whereby individuals with eyes having less anterior chamber depth and shorter axial length are at increased risk of PACG[36]. We examined the six loci associated with axial length at genome-wide significance previously reported in a large meta-analysis of 12,531 Europeans and 8,216 Asians[37] in our discovery GWAS for PACG. None of the associations (Supplementary Table 8) survived correction for multiple comparisons. We note nominal evidence of association with PACG at the *ABCC5* locus, which we previously reported[38] as being associated with anterior chamber depth (for SNP rs4148579, pairwise $r^2 = 0.99$ with the previously reported rs1401999; OR = 1.07, $P = 0.017$).

We then checked whether any of the five newly associated PACG loci directly underlie functional genomic elements. We observed that almost all of the sentinel SNPs as well as SNPs in linkage disequilibrium (LD) are located within potential transcription factor binding sites (Supplementary Table 9)[39,40,41]. None of the sentinel SNPs tag ($r^2 > 0.8$) any exonic SNPs in genes within the respective loci. Examination of recently available large-scale expression quantitative trait locus (eQTL) mapping databases[42,43] indicated that only SNPs

rs3739821 on chromosome 9 and rs7494379 on chromosome 14 are significant eQTLs in human tissues (Supplementary Table 10). However, the data may allow us to draw limited inferences, as rs3739821 has significant eQTL effects on *DPM2* ($P = 1.44 \times 10^{-12}$) and *FAM102A* ($P = 4.57 \times 10^{-6}$), as well as on the neighboring *ST6GALNAC6* ($P = 6.79 \times 10^{-20}$) and *ST6GALNAC4* ($P = 5.32 \times 10^{-6}$) genes[42]. Looking up our loci in a second eQTL database derived from gene expression analysis in blood cells[44], SNP rs3739821 has a significant eQTL effect on *ST6GALNAC4* in monocytes, associated with lower expression ($\beta = -0.1$, $P = 2.4 \times 10^{-8}$). Further work is needed to determine the functional effects of these variants on PACG susceptibility.

In summary, our expanded GWAS and replication study of PACG has identified five new susceptibility loci, thus bringing the total number of replicated loci to eight. These eight loci explain up to 1.8% of the overall disease variance in PACG, in line with observations for many complex diseases[45,46]. These results further reinforce the potential importance of cell–cell adhesion and collagen metabolism in PACG pathogenesis. Furthermore, our observations newly implicate acetylcholine metabolism, yet uncharacterized metabolic pathways mediated through zinc-finger activation and repression of transcription, and changes in glycosylation as candidate pathways for future work aimed at identifying the mechanisms responsible for PACG susceptibility.

Methods

Patient collections.

DNA samples from all PACG cases and controls were collected after written informed consent was obtained from each participant, strictly in accordance with the tenets of the Declaration of Helsinki. Details for each case–control collection are provided in the Supplementary Note.

Genotyping.

For the GWAS discovery stage, genome-wide genotyping was performed using the Illumina 610K/660W and OmniExpress BeadChips following the manufacturer's instructions and as previously described[1].

For the replication stage, the most significantly associated SNPs from the discovery stage were genotyped using Applied Biosystems TaqMan genotyping assays as well as the Sequenom MassARRAY system, as previously described[47]. We performed cross-platform concordance checks and verified > 99.9% concordance of genotypes for the SNP markers surpassing genome-wide significance reported here.

Statistical analysis.

Stringent quality checks were performed on a per-SNP and per-sample basis, with removal of SNPs showing a genotyping success rate of <95% or a MAF of <1%, as well as deviation from Hardy–Weinberg equilibrium ($P < 1 \times 10^{-6}$ for deviation). Samples were similarly checked, and those with a genotyping success rate of <95% were removed, as were those showing excesses heterozygosity and outliers on principal-component analysis of genetic ancestry. PACG cases were contrasted to ancestry- and geographically matched controls for each country strata, as is now routinely done in GWAS[48,49,50]. PACG cases and controls appeared to be well matched in terms of ancestry for each stratum, as well as in overall assessment (Fig. 1 and Supplementary Figs. 10 and 11). In the discovery stage, we analyzed a total of 745,080 SNPs with direct genotyping and > 4,500,000 SNPs with imputation. The relationship between each variable genetic SNP marker and PACG disease was measured using logistic regression with further adjustments for principal components of genetic stratification. We observed minimal overall genomic inflation in each of the discovery sample collections and in the discovery meta-analysis (overall λ_{GC} for the meta-analysis = 1.05; Supplementary Fig.

12 and Supplementary Table 1). We then performed a meta-analysis of all the discovery-stage PACG collections, summarizing the data across the 16 case–control strata (Supplementary Table 1) using random-effects meta-analysis. We used the random-effects model to provide for more robust estimation of *P* values and odds ratios in the discovery stage because of the ancestrally and geographically diverse patient collections. Such an approach allows us the best chance of identifying PACG susceptibility variants shared by most of the ancestry groups.

The biological relationships of all remaining samples were then verified using the principle of variability in allele sharing. Identity-by-state information from comparisons of each sample pair was derived using PLINK software (see URLs). For each pair of individuals showing evidence of cryptic relatedness (possibly due either to inadvertent sample duplication or biologically related samples), we excluded the sample with the lower call rate from further analysis. Principal-component analysis was then undertaken to minimize spurious associations due to ancestry differences between PACG cases and controls. Plots of principal components were generated using the R statistical package (see URLs).

For both the GWAS discovery and replication stages, the association between SNP genotypes and PACG disease status was measured using score-based tests (1 degree of freedom). These general tests model additive effects of the minor allele on disease risk. They do not assume any mode of inheritance and are well described elsewhere. Each SNP genotype is coded according to allele dosage: 0 for individuals with the wild-type genotype for a given SNP, 1 for individuals heterozygous for the alternate allele, and 2 for individuals homozygous for the alternate allele.

In the GWAS discovery stage, the association analysis was also adjusted for the principal components of genetic stratification for sample collections where residual population stratification existed. Details on the overall genomic inflation factor and number of principal components used for adjustment in each of the GWAS discovery collections are provided in Supplementary Table 1. The genome-wide association summary statistics for all SNP markers with direct microarray genotyping together with imputation fine-mapping of the significant loci are provided as the Supplementary Data Set.

As the replication stage only tested a limited number of SNP markers, we were unable to adjust for population stratification in this stage. Nonetheless, association tests were performed for each stratum separately, and the cohorts were subsequently combined in meta-analysis. Meta-analysis was conducted using inverse-variance weights for each PACG case–control collection, which calculates an overall *z* statistic, its corresponding *P* value, and accompanying odds ratios for each SNP analyzed. All *P* values reported here are two-tailed.

At each locus, the sentinel SNP is defined as the most significant directly genotyped SNP within that locus. Independent loci are defined as loci with no LD between them (pairwise $r^2 < 0.01$) and are located more than 1 Mb apart from one another.

Genotype imputation.

To improve the genetic resolution beyond that provided by the directly genotyped SNPs present on standard-content GWAS arrays, we performed imputation for the GWAS discovery sample collections using samples and SNP markers passing standard GWAS quality control checks. The imputation and phasing of genotypes were carried out using IMPUTE2 software (see URLs) with a reference panel constructed from cosmopolitan population haplotypes based on data obtained for 2,535 individuals from 26 distinct populations around the world. These data are part of the 1000 Genomes Project Phase 3 (June 2014) release. Imputed genotypes were called with an IMPUTE probability threshold of 0.90, with all other genotypes classified as missing. We

applied additional quality control filters to exclude SNP markers with a call rate of <99% should the SNP have a MAF of <5% in either cases or controls. For common SNPs with MAF > 5%, the filtering criterion was set to exclude SNPs with a call rate of <95%.

Power calculation.

All statistical power calculations were performed as previously described for two-stage GWAS and replication studies[50]. We present these power calculations for each of the following conditions: (i) GWAS discovery stage only and (ii) GWAS discovery and replication stages (Supplementary Table 4).

Expression analysis.

Expression of *EPDR1*, *GLIS3*, *DPM2*, *FAM102A*, *PIP5KL1*, and *FERMT2* was assessed by semiquantitative RT–PCR using gene-specific primers (Supplementary Table 11) on the following human ocular tissues: sclera, cornea, lens with lens capsule, iris, trabecular meshwork, ciliary body, retina, choroid, optic nerve head, and optic nerve. Human donor eyes were obtained from the Florida Lions Eye Banks and dissected into respective ocular regions for RNA extraction and semiquantitative RT–PCR expression analysis. Ethical approval for this section of the study was granted by the Institutional Review Board of the Singapore Eye Research Institute for donor eyes procured from the Florida Lions Eye Bank. All of the investigated genes produced multiple transcripts through alternative splicing that resulted in several protein isoforms. In this study, we investigated the mRNA expression of the full-length or leading transcript that produced the 'canonical' protein isoform (Supplementary Table 11). The NCBI reference sequence from which the primer sequences were derived is indicated for each gene. Primers were selected specifically to target the mRNA and not the genomic DNA of the genes examined. All gene-specific primers therefore spanned an intron, and the sizes of the PCR products obtained (*EPDR1*, 210 bp; *GLIS3*, 247 bp; *DPM2*, 218 bp; *FAM102A*, 155 bp; *PIP5KL1*, 189 bp; *FERMT2*, 159 bp) confirmed the amplification of mRNA. We were unable to successfully amplify a specific PCR product for the *CHAT* gene despite multiple attempts. The ocular expression of CHAT protein was therefore investigated through immunoblot and immunohistochemistry analyses in ocular tissues. Total RNA was extracted from a variety of ocular tissues (sclera, cornea, iris, trabecular meshwork, ciliary body, lens and capsule, retina, choroid, optic nerve head, and optic nerve) with TRIzol reagent (Invitrogen) in accordance with the manufacturer's protocol. First-strand cDNA synthesis was performed with the SuperScript First-Strand Synthesis System for RT–PCR (Invitrogen) using random primers. Semiquantitative RT–PCR was performed according to the manufacturer's protocol, with SYBR Green Mastermix (Invitrogen) using the specified gene primers and equal amounts of cDNA template. The resulting PCR products were separated on a 2% agarose gel and visualized by ethidium bromide staining. The ubiquitously expressed β-actin (*ACTB*) gene (primers listed in Supplementary Table 11) was used as an amplification and normalizing control. All RT–PCR products were resequenced to confirm that the correct template was targeted by the primer pair selected for each gene. Semiquantitative RT–PCR was performed in triplicate to confirm the expression results, and a representative image of each agarose gel is shown.

Immunoblotting.

A human non-pigmented ciliary epithelial (NPCE) cell line was provided by M. Coca-Prados (Yale School of Medicine); a human trabecular meshwork (HTM) cell line was purchased from PromoCell; and a human cervical adenocarcinoma cell line (HeLa S), a human breast adenocarcinoma cell line (MCF-7), and a human embryonic kidney epithelial cell line (HEK293) together with a human retinal pigment epithelial cell line (APRE-19) were obtained from the American Type Culture Collection. All cell lines were tested for mycoplasma and were found to be negative. Cell lysates were generated by lysing individual cell lines with lysis buffer (50 mM Tris-HCl, pH 8, 150 mM NaCl, 1.0% Nonidet P-40, 0.5% deoxycholate, 0.1% SDS, 0.2 mM sodium orthovanadate, 10 mM sodium fluoride, 0.4 mM EDTA, and 10% glycerol). Proteins were resolved by SDS–PAGE and transferred to HyBond-C Extra nitrocellulose membranes (Amersham Life Science). Membranes were blocked in 5% nonfat milk with 10% BSA and 0.1% Tween-20 in Tris-buffered

saline (20 mM Tris-HCl, pH 7.6 and 150 mM NaCl) for 1 h before incubation with antibody to choline acetyltransferase (1:500 dilution) from Pierce (PA1-9027; RI); antibody to ependymin-related protein 1 (zebrafish) (EPDR1) (1:500 dilution) from antibodies-online (AA 38-225); antibody to GLIS3 (1:250 dilution) from Sigma-Aldrich (HPA056426); antibody to FERMT2 (1:250 dilution) from Sigma-Aldrich (HPA040505); antibody to DPM2 (1:250 dilution) from Sigma-Aldrich (SAB1104864); antibody to FAM102A (1:250 dilution) from Novus Biologicals (NBP1-88808); antibody to PIP5KL1 (1:250 dilution) from Novus Biologicals (NBP2-29992); and antibody to GAPDH (1:50,000 dilution) from Santa Cruz Biotechnology (sc-25778). Blocking and blotting with antibodies were performed in 5% nonfat milk with 10% BSA and 0.1% Tween-20 in PBS for 1 h each. Horseradish peroxidase (HRP)-conjugated secondary antibodies (GE Healthcare Biosciences) were applied to detect the bound primary antibodies, and signal was visualized with Luminata Forte Western HRP substrate (Millipore).

Immunofluorescence confocal microscopy of tissue sections.

Three archival human enucleated eye globes from Singapore (Singapore General Hospital–SNEC Ophthalmic Pathology Service, SGH Department of Pathology) were retrieved for immunofluorescence analysis as normal controls. Ethical approval was provided by the Singapore Health Services Centralized Institutional Review Board. These globes were enucleated for other pathological diagnoses and did not have any intraocular disease. Immunofluorescence analysis was performed according to our previously published protocol6. Briefly, paraffin sections were cut at 4 μm and fished onto coated slides, before being dewaxed. Antigen retrieval was performed using Leica Bond ER2 solution for 20 min at 100 °C. Tissue sections were then blocked using 10% FBS and 0.1% Tween-20 in PBS with 1× penicillin-streptomycin for 1 h at room temperature. All primary antibodies were diluted by 1:100 with blocking buffer and incubated with sections overnight at 4 °C. Sections were subsequently labeled with FITC-conjugated (1:300 dilution) anti-mouse, anti-rabbit, or anti-goat secondary antibody (Jackson Laboratories), followed by application of Vectashield with DAPI (Vector Laboratories). Stained histology sections were then coverslipped and stored in the dark at 4 °C. Images were acquired with a Leica TCS SP8 confocal microscope (Leica Microsystems) at the Advanced Bioimaging Core at the Academia, Singapore Health Services.

Acknowledgements
This research is supported by the Singapore Ministry of Health's National Medical Research Council under its Translational and Clinical Research (TCR) Flagship Programme Grant Stratified Medicine for Primary Angle Closure Glaucoma (NMRC/TCR/008-SERI/2013) and the Singapore Translational Research (STaR) Investigator Award Singapore Angle Closure Glaucoma Program Characterization, Prevention, and Management (NMRC/STAR/0023/2014), as well as the Biomedical Research Council, Agency for Science, Technology and Research (A-STAR), Singapore. A.T.L.-S. gratefully acknowledges support from grants RUI 1001/PPSP/812101 and RUI 1001/PPSP/812152 from the Universiti Sains Malaysia. H.J., C.Q., and N. Wang acknowledge support from the Program of Beijing Scholars (2013), Leading Talents–High-Level Talents of the Health System of Beijing (2009-1-05), and the National Major Scientific and Technological Special Project for 'Significant New Drugs Development' (2011ZX09302-007-05), as well as Project of the National Natural Science Foundation of China (81570837) grants.

Author information
Author notes
Chiea Chuen Khor, Tan Do, Hongyan Jia, Masakazu Nakano, Ronnie George, Khaled Abu-Amero, Roopam Duvesh and Li Jia Chen: These authors contributed equally to this work.

Nhu Hon Do, Periasamy Sundaresan, Clement C Tham, Paul J Foster, Lingam Vijaya, Kei Tashiro, Eranga N Vithana, Ningli Wang and Tin Aung: These authors jointly directed this work.

Ethics declarations

Competing interests

The authors declare no competing financial interests.

Reference

1. Vithana, E.N. *et al.* Genome-wide association analyses identify three new susceptibility loci for primary angle closure glaucoma. *Nat. Genet.* **44**, 1142–1146 (2012).
2. Thylefors, B., Négrel, A.D., Pararajasegaram, R. & Dadzie, K.Y. Global data on blindness. *Bull. World Health Organ.* **73**, 115–121 (1995).
3. Hysi, P.G. *et al.* Genome-wide analysis of multi-ancestry cohorts identifies new loci influencing intraocular pressure and susceptibility to glaucoma. *Nat. Genet.* **46**, 1126–1130 (2014).
4. Gharahkhani, P. *et al.* Common variants near *ABCA1*, *AFAP1* and *GMDS* confer risk of primary open-angle glaucoma. *Nat. Genet.* **46**, 1120–1125 (2014).
5. Wiggs, J.L. *et al.* Common variants at 9p21 and 8q22 are associated with increased susceptibility to optic nerve degeneration in glaucoma. *PLoS Genet.* **8**, e1002654 (2012).
6. Aung, T. *et al.* A common variant mapping to *CACNA1A* is associated with susceptibility to exfoliation syndrome. *Nat. Genet.* **47**, 387–392 (2015).
7. Foster, P.J., Buhrmann, R., Quigley, H.A. & Johnson, G.J. The definition and classification of glaucoma in prevalence surveys. *Br. J. Ophthalmol.* **86**, 238–242 (2002).
8. Cheng, J.W., Zong, Y., Zeng, Y.Y. & Wei, R.L. The prevalence of primary angle closure glaucoma in adult Asians: a systematic review and meta-analysis. *PLoS One* **9**, e103222 (2014).
9. Quigley, H.A. & Broman, A.T. The number of people with glaucoma worldwide in 2010 and 2020. *Br. J. Ophthalmol.* **90**, 262–267 (2006).
10. Foster, P.J. & Johnson, G.J. Glaucoma in China: how big is the problem? *Br. J. Ophthalmol.* **85**, 1277–1282 (2001).
11. Foster, P.J. *et al.* The prevalence of glaucoma in Chinese residents of Singapore: a cross-sectional population survey of the Tanjong Pagar district. *Arch. Ophthalmol.* **118**, 1105–1111 (2000).
12. Dandona, L. *et al.* Angle-closure glaucoma in an urban population in southern India. The Andhra Pradesh eye disease study. *Ophthalmology* **107**, 1710–1716 (2000).
13. Quigley, H.A., Congdon, N.G. & Friedman, D.S. Glaucoma in China (and worldwide): changes in established thinking will decrease preventable blindness. *Br. J. Ophthalmol.* **85**, 1271–1272 (2001).
14. Purdue, M.P. *et al.* Genome-wide association study of renal cell carcinoma identifies two susceptibility loci on 2p21 and 11q13.3. *Nat. Genet.* **43**, 60–65 (2011).
15. International Parkinson Disease Genomics Consortium. Imputation of sequence variants for identification of genetic risks for Parkinson's disease: a meta-analysis of genome-wide association studies. *Lancet* **377**, 641–649 (2011).
16. Ellinor, P.T. *et al.* Meta-analysis identifies six new susceptibility loci for atrial fibrillation. *Nat. Genet.* **44**, 670–675 (2012).
17. Gudbjartsson, D.F. *et al.* A sequence variant in *ZFHX3* on 16q22 associates with atrial fibrillation and ischemic stroke. *Nat. Genet.* **41**, 876–878 (2009).
18. Pomerantz, M.M. *et al.* The 8q24 cancer risk variant rs6983267 shows long-range interaction with *MYC* in colorectal cancer. *Nat. Genet.* **41**, 882–884 (2009).
19. Tuupanen, S. *et al.* The common colorectal cancer predisposition SNP rs6983267 at chromosome 8q24 confers potential to enhanced Wnt signaling. *Nat. Genet.* **41**, 885–890 (2009).
20. Gregorio-King, C.C. et al. MERP1: a mammalian ependymin-related protein gene differentially expressed in hematopoietic cells. Gene 286, 249–257 (2002).
21. Dolmans, G.H. et al. Wnt signaling and Dupuytren's disease. N. Engl. J. Med. 365, 307–317 (2011).
22. Barone, R. et al. DPM2-CDG: a muscular dystrophy–dystroglycanopathy syndrome with severe epilepsy. Ann. Neurol. 72, 550–558 (2012).
23. Wang, D.Y., Fulthorpe, R., Liss, S.N. & Edwards, E.A. Identification of estrogenresponsive genes by complementary deoxyribonucleic acid microarray and characterization of a novel early estrogen-induced gene: EEIG1. Mol. Endocrinol. 18, 402–411 (2004).
24. Shi, L. et al. Overexpression of PIP5KL1 suppresses cell proliferation and migration in human gastric cancer cells. Mol. Biol. Rep. 37, 2189–2198 (2010).
25. Lachkar, Y. & Bouassida, W. Drug-induced acute angle closure glaucoma. Curr. Opin. Ophthalmol. 18, 129–133 (2007).
26. Mandak, J.S., Minerva, P., Wilson, T.W. & Smith, E.K. Angle closure glaucoma complicating systemic atropine use in the cardiac catheterization laboratory. Cathet. Cardiovasc. Diagn. 39, 262–264 (1996).

27. Shen, Z. et al. Novel focal adhesion protein kindlin-2 promotes the invasion of gastric cancer cells through phosphorylation of integrin β1 and β3. J. Surg. Oncol. 108, 106–112 (2013).
28. Kim, Y.S., Nakanishi, G., Lewandoski, M. & Jetten, A.M. GLIS3, a novel member of the GLIS subfamily of Krüppel-like zinc finger proteins with repressor and activation functions. Nucleic Acids Res. 31, 5513–5525 (2003)
29. Senée, V. et al. Mutations in GLIS3 are responsible for a rare syndrome with neonatal diabetes mellitus and congenital hypothyroidism. Nat. Genet. 38, 682–687 (2006).
30. Barrett, J.C. et al. Genome-wide association study and meta-analysis find that over 40 loci affect risk of type 1 diabetes. Nat. Genet. 41, 703–707 (2009).
31. Cho, Y.S. et al. Meta-analysis of genome-wide association studies identifies eight new loci for type 2 diabetes in east Asians. Nat. Genet. 44, 67–72 (2012).
32. Dupuis, J. et al. New genetic loci implicated in fasting glucose homeostasis and their impact on type 2 diabetes risk. Nat. Genet. 42, 105–116 (2010).
33. Burdon, K.P. et al. Genome-wide association study identifies susceptibility loci for open angle glaucoma at TMCO1 and CDKN2B-AS1. Nat. Genet. 43, 574–578 (2011).
34. Chen, Y. et al. Common variants near ABCA1 and in PMM2 are associated with primary open-angle glaucoma. Nat. Genet. 46, 1115–1119 (2014).
35. Li, Z. et al. A common variant near TGFBR3 is associated with primary open angle glaucoma. Hum. Mol. Genet. 24, 3880–3892 (2015).
36. Nongpiur, M.E. et al. Lack of association between primary angle-closure glaucoma susceptibility loci and the ocular biometric parameters anterior chamber depth and axial length. Invest. Ophthalmol. Vis. Sci. 54, 5824–5828 (2013).
37. Cheng, C.Y. et al. Nine loci for ocular axial length identified through genome-wide association studies, including shared loci with refractive error. Am. J. Hum. Genet. 93, 264–277 (2013).
38. Nongpiur, M.E. et al. ABCC5, a gene that influences the anterior chamber depth, is associated with primary angle closure glaucoma. PLoS Genet. 10, e1004089 (2014).
39. Boyle, A.P. et al. Annotation of functional variation in personal genomes using RegulomeDB. Genome Res. 22, 1790–1797 (2012).
40. Ward, L.D. & Kellis, M. HaploReg: a resource for exploring chromatin states, conservation, and regulatory motif alterations within sets of genetically linked variants. Nucleic Acids Res. 40, D930–D934 (2012).
41. ENCODE Project Consortium. An integrated encyclopedia of DNA elements in the human genome. Nature 489, 57–74 (2012).
42. Westra, H.J. et al. Systematic identification of trans eQTLs as putative drivers of known disease associations. Nat. Genet. 45, 1238–1243 (2013).
43. GTEx Consortium. The Genotype-Tissue Expression (GTEx) project. Nat. Genet. 45, 580–585 (2013).
44. Fairfax, B.P. et al. Genetics of gene expression in primary immune cells identifies cell type–specific master regulators and roles of HLA alleles. Nat. Genet. 44, 502–510 (2012).
45. Okada, Y. et al. Genetics of rheumatoid arthritis contributes to biology and drug discovery. Nature 506, 376–381 (2014).
46. Speliotes, E.K. et al. Association analyses of 249,796 individuals reveal 18 new loci associated with body mass index. Nat. Genet. 42, 937–948 (2010).
47. Dunstan, S.J. et al. Variation at HLA-DRB1 is associated with resistance to enteric fever. Nat. Genet. 46, 1333–1336 (2014).
48. Verhoeven, V.J. et al. Genome-wide meta-analyses of multiancestry cohorts identify multiple new susceptibility loci for refractive error and myopia. Nat. Genet. 45, 314–318 (2013).
49. Al Olama, A.A. et al. A meta-analysis of 87,040 individuals identifies 23 new susceptibility loci for prostate cancer. Nat. Genet. 46, 1103–1109 (2014).
50. Kiryluk, K. et al. Discovery of new risk loci for IgA nephropathy implicates genes involved in immunity against intestinal pathogens. Nat. Genet. 46, 1187–1196 (2014).

Figure

Figure 1: Distribution of PACG cases and controls from the GWAS discovery stage, which encompassed collections from 15 countries.

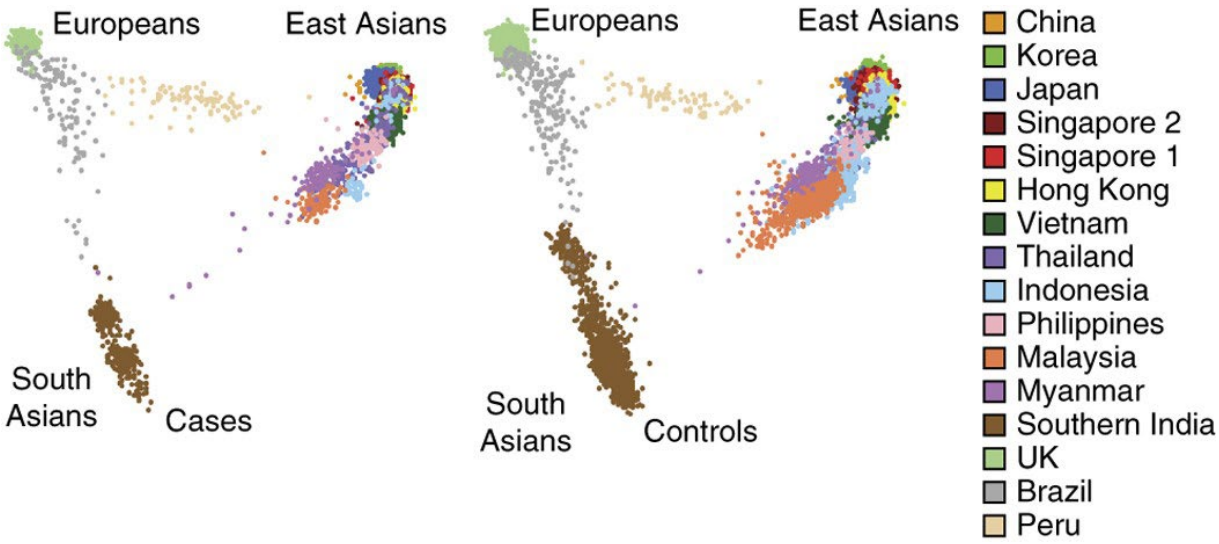

Cases and controls are projected onto the top two principal components of genetic stratification, with cases on the left and controls on the right. Principal-component comparisons for each of the East Asian countries are shown in Supplementary Figure 10.

Figure 2: Results of the discovery GWAS meta-analysis.

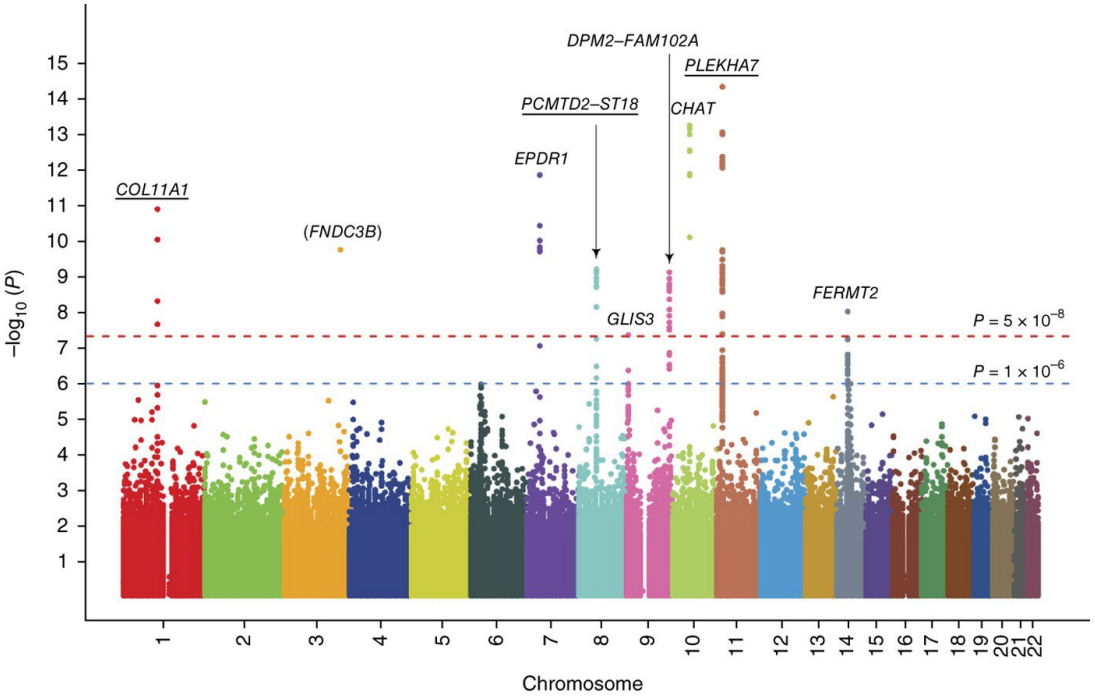

The three previously reported loci are underlined. *FNDC3B* did not replicate in the replication collections. SNPs at *EPDR1*, *GLIS3*, *DPM2–FAM102A*, *CHAT*, and *FERMT2* represent new genome-wide significant associations.

Figure 3: Forest plots for the five new genome-wide significant loci.

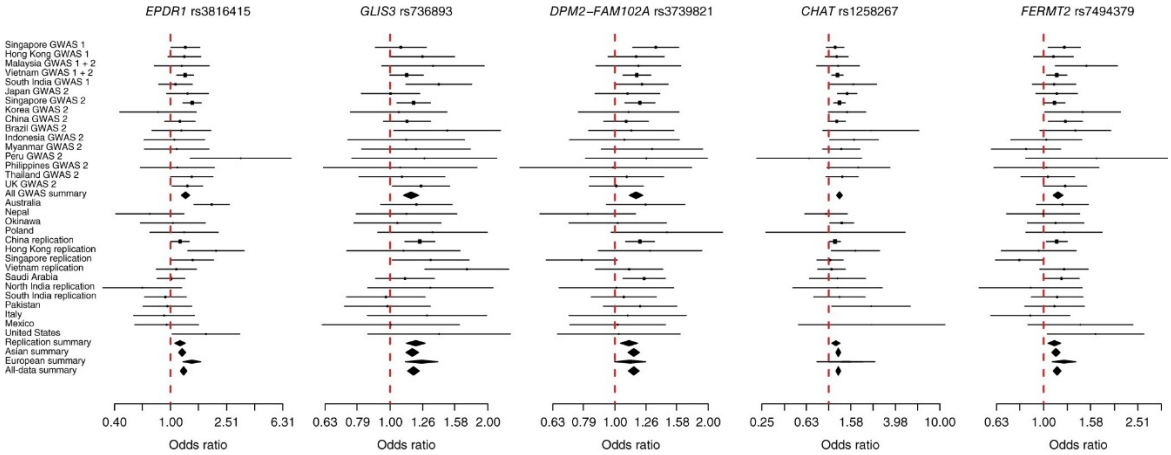

Point estimates for each locus are denoted as risk allele odds ratios, accompanied by horizontal lines representing the 95% confidence interval for each point estimate. Diamonds represent meta-analyses for the GWAS discovery stage, replication stage, all Asians, and all Europeans, as well as for all samples. The vertical dashed red line represents an OR of 1.00, indicating no effect.

Table

Table 1 Results for the eight genome-wide significant loci upon meta-analysis of all PACG case–control collections

SNP (risk/reference)	Chr.	Position (bp)	Gene locus	Stage	Per-allele OR	*P*	P_{het}	I^2 index (%)
New loci								
rs3816415 (A/G)	7	37,988,311	*EPDR1*	GWAS	1.28	1.28×10^{-12}	0.6	0
				Replication	1.17	0.00032	0.0013	60.4
				All-data meta-analysis	1.24	5.94×10^{-15}	0.0072	43.0
				Asian descent	1.21	7.49×10^{-11}	0.095	29.1
				European descent	1.42	1.86×10^{-6}	0.029	55.3
rs736893 (G/A)	9	4,217,028	*GLIS3*	GWAS	1.16	4.23×10^{-8}	0.85	0
				Replication	1.20	4.64×10^{-8}	0.48	0
				All-data meta-analysis	1.18	1.43×10^{-14}	0.78	0
				Asian descent	1.17	1.2×10^{-11}	0.57	0
				European descent	1.25	0.00015	0.94	0

SNP (risk/reference)	Chr.	Position (bp)	Gene locus	Stage	Per-allele OR	*P*	P_{het}	I^2 index (%)
rs3739821 (G/A)	9	130,702,477	*DPM2–FAM102A*	GWAS	1.17	7.08×10^{-10}	0.93	0
				Replication	1.11	0.0013	0.28	15.7
				All-data meta-analysis	1.15	8.32×10^{-12}	0.62	0
				Asian descent	1.15	4.5×10^{-11}	0.46	0
				European descent	1.12	0.06	0.79	0
rs1258267 (A/G)	10	50,895,770	*CHAT*	GWAS	1.25	5.06×10^{-14}	0.59	0
				Replication	1.16	0.00046	0.57	0
				All-data meta-analysis	1.22	2.85×10^{-16}	0.58	0
				Asian descent	1.22	4.99×10^{-16}	0.58	0
				European descent	1.43	0.24[a]	0.32	14.2
rs7494379 (G/A)	14	53,411,391	*FERMT2*	GWAS	1.15	9.26×10^{-9}	0.56	0
				Replication	1.11	0.00065	0.24	19.2
				All-data meta-analysis	1.14	3.43×10^{-11}	0.39	5.0

SNP (risk/reference)	Chr.	Position (bp)	Gene locus	Stage	Per-allele OR	*P*	P_{het}	I^2 index (%)
				Asian descent	1.13	5.42×10^{-9}	0.36	7.3
				European descent	1.22	0.00066	0.52	0
Previously reported loci								
rs3753841 (G/A)	1	103,379,918	*COL11A1*	GWAS	1.18	1.18×10^{-11}	0.32	11.4
				Replication	1.29	1.15×10^{-14}	0.47	0
				All-data meta-analysis	1.21	1.27×10^{-23}	0.21	16.8
				Asian descent	1.21	4×10^{-21}	0.35	8.1
				European descent	1.20	0.00076	0.099	42.0
rs1015213 (A/G)	8	52,887,541	*PCMTD1–ST18*	GWAS	1.44	1.75×10^{-9}	0.21	21.2
				Replication	1.40	5.47×10^{-8}	0.51	0
				All-data meta-analysis	1.42	5.42×10^{-16}	0.34	8.0
				Asian descent	1.44	1.68×10^{-13}	0.096	29
				European descent	1.35	0.0006	0.99	0

SNP (risk/reference)	Chr.	Position (bp)	Gene locus	Stage	Per-allele OR	*P*	P_{het}	I^2 index (%)
rs11024102 (G/A)	11	17,008,605	*PLEKHA7*	GWAS	1.20	4.1×10^{-15}	0.77	0
				Replication	1.15	5.51×10^{-5}	0.48	0
				All-data meta-analysis	1.18	1.93×10^{-18}	0.71	0
				Asian descent	1.20	8×10^{-19}	0.87	0
				European descent	1.05	0.38	0.54	0

1. All SNPs reported here were directly genotyped on the GWAS arrays. Chr., chromosome.
2. [a]The minor allele for *CHAT* rs1258267 is very rare in Europeans (Supplementary Table 5). Of the six European-ancestry populations (Australia, Brazil, Peru, Poland, UK, and United States), only those from Brazil, Peru, and Poland had MAF >1% and thus could be tested for genetic association.

Integrated supplementary information

Accession codes.

The genome-wide association summary statistics for all SNP markers with direct microarray genotyping together with imputation fine-mapping of the significant loci are provided as the Supplementary Data Set.

Supplementary Figure 1 Regional association analysis for the five newly identified loci surpassing genome-wide significance.
The horizontal axis represents physical distance in megabases on hg37 coordinates. The vertical axis of the left represents –log10 (P values) for association with PACG. The vertical axis on the right represents the recombination rate in centiMorgans and is taken from the HapMap panels.

Supplementary Figure 2 Ocular expression of genes at PACG-associated loci.
(a) Expression analysis of EPDR1, GLIS3, DPM2, FAM102A, FERMT2, and PIP5KL1 in human ocular tissues by RT-PCR using gene-specific primers (Supplementary Table 9). RT-PCR products were observed differentially in sclera (S), cornea (Co), lens with lens capsule (L), iris (I), trabecular meshwork (TM), ciliary body (CB), retina (R), choroid (Ch), optic nerve head (ONH), and optic nerve (ON). The ubiquitously expressed gene ACTB was used as the normalizing control. A no-template sample acted as the negative control (NC) to ensure no contamination of the RT-PCR reaction mix. M denotes the molecular weight marker. (b–h) Immunoblots of whole-cell lysates from retinal pigment epithelial (ARPE19), non-pigmented ciliary epithelial (NPCE), human trabecular meshwork (HTM), human cervical adenocarcinoma (Hela S), human breast adenocarcinoma (MCF7), and human embryonic kidney epithelial (HEK 293) cells, probed for CHAT, EPDR1, GLIS3, DPM2, FAM102A, FERMT2, and PIP5KL1 proteins and GAPDH, as a loading control. The protein isoforms detected by the respective antibodies were CHAT (83 kDa), EPDR1 (~25 kDa and ~18 kDa corresponding to two alternatively spliced forms of EPDR1), GLIS3 (~118 kDa and 90 kDa corresponding to two alternatively spliced forms of GLIS3), DPM2 (~17 kDa), FAM102A (37 kDa), FERMT2 (~78 kDa), and PIP5KL1 (22 kDa). The arrowheads indicate specific protein bands.

Supplementary Figure 3 Analysis of CHAT distribution in human ocular tissues.
(a) Strong diffuse immunoreactivity of CHAT was detected in the posterior iris epithelium (PIE) and anterior iris border (AIB). In the iris stroma (IS), the iris stromal cells also show moderate to strong positive staining for CHAT, whereas the iris dilator muscle shows only weak and variable immunoreactivity. (b) In the ciliary body, pronounced yet diffuse staining of CHAT was detected in the pigmented ciliary epithelium (PCE). (c) The ciliary muscles (CM) showed strong and diffuse staining of the CHAT protein, whereas more moderate immunoreactivity was detected in the trabecular meshwork (TM) along the trabecular beams. (d,e) The corneal epithelium (C. Epi) and Descemet's membrane (Descemet's) demonstrated positive immunoreactivity for CHAT in contrast to the negative staining in stromal keratocytes, corneal stroma (C. Stroma), and endothelial cells (C. Endo). (f) In the retina, CHAT expression was diffusely and strongly positive in photoreceptors (PR). Negative immunoreactivity was seen in the nerve fiber layer, ganglion cell layer (GCL) inner plexiform layer, inner nuclear layer (INL), outer plexiform layer, and outer nuclear layer (ONL).

Supplementary Figure 4 Analysis of EPDR1 distribution in human ocular tissues.
(a) In the iris, diffuse and strong immunoreactivity for EPDR1 was seen throughout the iris tissue. These areas included the posterior iris epithelium (PIE), iris dilator muscle (IDM), cells within the iris stroma (IS) as well as the iris capillaries (IC), and anterior iris border (AIB). (b) In the ciliary body, EPDR1 protein expression was detected as diffuse and strongly positive immunoreactivity in ciliary body vessels (CBV) and non-pigmented ciliary epithelium (NPCE). Although positive staining was detected in pigmented ciliary epithelium (PCE), the intensity was weaker than those for NPCE and CBV. (c) EPDR1 protein was also expressed throughout the trabecular meshwork (TM) and Schlemm's canal (SC). (d,e) In the cornea, EPDR1 was detected

in the cornea epithelium (C. Epi.) and cornea endothelial (C. Endo) layers. (f) In the retina, EPDR1 staining was detected in the nerve fiber layer (NFL), ganglion cell layer (GCL), inner plexiform layer (IPL), outer plexiform layer (OPL), and photoreceptors (PR).

Supplementary Figure 5 Analysis of FERMT2 distribution in human ocular tissues.
(a) In the iris, strong and diffuse FERMT2 immunoreactivity was detected in the iris dilator muscle (IDM). Moderate to strong immunoreactivity was also seen in cells within the iris stroma (IS) and iris capillaries (IC), whereas the anterior iris border showed only moderate immunoreactivity. (b) In the ciliary body, strong FERMT2 expression was detected in both non-pigmented ciliary epithelium (NPCE) and pigmented ciliary epithelium (PCE). (c) Strong FERMT2 immunoreactivity was detected in the ciliary muscles (CM), trabecular meshwork (TM), and Schlemm's canal (SC). (d,e) In the cornea, FERMT2 expression was observed in cornea epithelium (C. Epi.) and cornea endothelium (C. Endo.). (f) In the retina, FERMT2 was variably expressed in the retinal layers, with strong and diffuse immunoreactivity detected in the photoreceptors (PR) and moderate immunoreactivity seen in the outer plexiform layer (OPL).

Supplementary Figure 6 Analysis of GLIS3 distribution in human ocular tissues.
(a) In the iris, GLIS3 showed strong and diffuse immunoreactivity in iris dilator muscle (IDM) and the anterior iris border (AIB). A positive punctate membranous staining pattern in addition to weaker cytoplasmic staining was observed in posterior pigment epithelium of the posterior iris epithelium (PIE). The cells in the iris stroma (IS) also demonstrated strong positive GLIS3 immunoreactivity. (b) GLIS3 protein expression was prominently seen in the ciliary muscle (CM). Strong and diffuse immunoreactivity was detected in the non-pigmented ciliary epithelium (NPCE), pigmented ciliary epithelium (PCE), and ciliary muscle (CM). (c) In the trabecular meshwork (TM) and Schlemm's canal (SC), strong and diffuse immunoreactivity was detected. (d,e) In the cornea, GLIS3 expression was detected in the cornea epithelium (C. Epi.) and cornea endothelium (C. Endo.). (f) In the retina, distinct strong and diffuse GLIS3 immunoreactivity was detected in the photoreceptors (PR) and outer plexiform layer (OPL), with much weaker variable immunoreactivity detected in the ganglion cell layer (GCL).

Supplementary Figure 7 Analysis of DPM2 distribution in human ocular tissues.
(a) In the iris, strong DPM2 expression was detected in the anterior iris border (AIB), cells within the iris stroma (IS), and iris capillaries (IC), with only moderate intensity of DPM2 immunostaining detected in iris dilator muscle (IDM). (b) DPM2 protein was found to be diffusely expressed in the ciliary body. Strong immunoreactivity was detected in both non-pigmented ciliary epithelium (NPCE) and pigmented ciliary epithelium (PCE), ciliary body blood vessels (CBV), and also ciliary muscle (CM). (c) DPM2 immunoreactivity was seen in trabecular meshwork (TM) and Schlemm's canal (SC). (d,e) In the cornea, DPM2 expression was observed in cornea stromal (C. stroma) collagen fibers but not keratocytes. Immunoreactivity to DPM2 was also seen in the cornea epithelium (C. Epi) and cornea endothelium (C. Endo.) IDM. (f) In the retina, strong and diffuse immunoreactivity of DPM2 was detected in the photoreceptors (PR) in contrast to the much weaker immunoreactivity seen in the outer plexiform layer (OPL) and the ganglion cell layer (GCL).

Supplementary Figure 8 Analysis of PIP5KL1 distribution in human ocular tissues.
(a) In the iris, pronounced and diffuse staining of PIP5KL1 was detected in the iris dilator muscle (IDM). Strong immunoreactivity was also seen in iris stromal cells (IS) and iris capillaries (IC). (b) PIP5KL1 expression was diffuse with strong positive staining observed in the non-pigmented ciliary epithelium (NPCE). A weaker staining profile was observed in pigmented ciliary epithelium (PCE), which is constrained to PCE cell–cell borders. (c) In the trabecular meshwork (TM) and Schlemm's canal (SC), strong immunoreactivity of PIP5KL1 was detected in TM beams and endothelial cells of the Schlemm's canal. (d,e) In the cornea, PIP5KL1 was strongly expressed in the nuclei and cytoplasm of the corneal epithelium (C. Epi.). Positive staining of stromal keratocytes was also seen. The corneal endothelium (C. Endo) showed intense

immunoreactivity to PIP5KL1. (f) In the retina, PIP5KL1 immunoreactivity in the outer limiting membrane (OLM) was distinctly prominent in comparison to the rest of the retinal layers. Similarly, the ganglion cell layer (GCL) also showed strong nuclear positive staining for PIP5KL1. In contrast, mild to moderate variable expression of PIP5KL1 protein was seen in photoreceptors (PR). Weak and variable immunoreactivity could be seen in the inner plexiform layer (IPL) and the inner nuclear layer (INL). The rest of the retina showed no significant immunoreactivity to PIP5KL1.

Supplementary Figure 9 Analysis of FAM102A distribution in human ocular tissues.
(a) In the iris, strong immunoreactivity of FAM102A protein was seen in the anterior iris border (AIB), iris stromal cells (IS), and the iris dilator muscle (IDM). Moderate and punctate staining of the posterior border of the posterior pigment epithelium portion of the posterior iris epithelium (PIE) was also seen. (b) In the ciliary body, strong immunoreactivity for FAM102A protein was limited to pigmented ciliary epithelium (PCE) and non-pigmented ciliary epithelium (NPCE), with PCE having stronger immunoreactivity. (c) Moderate immunoreactivity of FAM102A was observed in the trabecular meshwork (TM), Schlemm's canal (SC), and ciliary muscle (CM). (d,e) In cornea, only the basal epithelial layer of the cornea epithelium (C. Epi.) and corneal endothelial cells (C. Endo.) showed moderate FAM102A protein immunoreactivity. (f) In the retina, strong FAM102A immunoreactivity was distinctly localized to the outer limiting membrane (OLM), photoreceptors (PR), and nuclei of the ganglion cell layer (GCL). Patchy moderate immunoreactivity of FAM102A was also noted in the outer plexiform layer (OPL). The rest of the retinal layers showed no significant immunoreactivity to FAM102A.

Supplementary Figure 10 Distribution of PACG cases and controls of East Asian descent from the GWAS discovery stage.
PACG cases and controls are projected onto the top two principal components of genetic stratification, with cases on the left panel and controls on the right panel.

Supplementary Figure 11 Detailed ancestry analysis of PACG cases and controls from the GWAS discovery stage, which encompassed collections from 15 countries.
(a-f) The genetic principal components (PCs) for cases and controls are projected onto PC1 vs. PC3 (a), PC1 vs. PC4 (b), PC1 vs. PC5 (c), PC2 vs. PC3 (d), PC3 vs. PC4 (e), and PC4 vs PC5 (f). For each panel, PACG cases are projected on the left and controls on the right.

Supplementary Figure 12 Quantile-quantile plot showing the association results for the GWAS discovery stage encompassing 6,525 PACG cases and 19,929 controls.
Supplementary information
Supplementary Text and Figures
Supplementary Figures 1–12, Supplementary Note and Supplementary Tables 1–8, 10 and 11. (PDF 5580 kb)

Supplementary Table 9
Variants located within predicted regulatory regions and in LD (r2 >0.8) with the top SNPs in the five newly identified loci. (XLSX 29 kb)

Supplementary Data Set
Summary association statistics of the PACG GWAS SNPs with direct microarray genotyping together with imputation fine-mapping of the genome-wide significant loci. (TXT 29091 kb)

Supplementary Figure 1

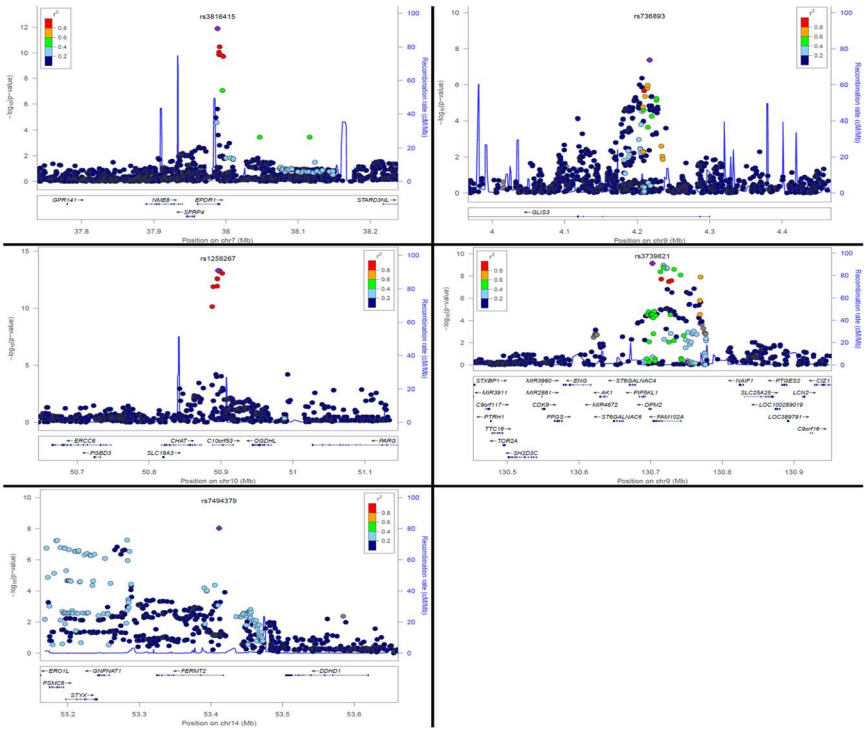

Regional association analysis for the five newly identified loci surpassing genome-wide significance.

The horizontal axis represents physical distance in megabases on hg37 coordinates. The vertical axis of the left represents $-\log_{10}$ (*P* values) for association with PACG. The vertical axis on the right represents the recombination rate in centiMorgans and is taken from the HapMap panels.

Supplementary Figure 2

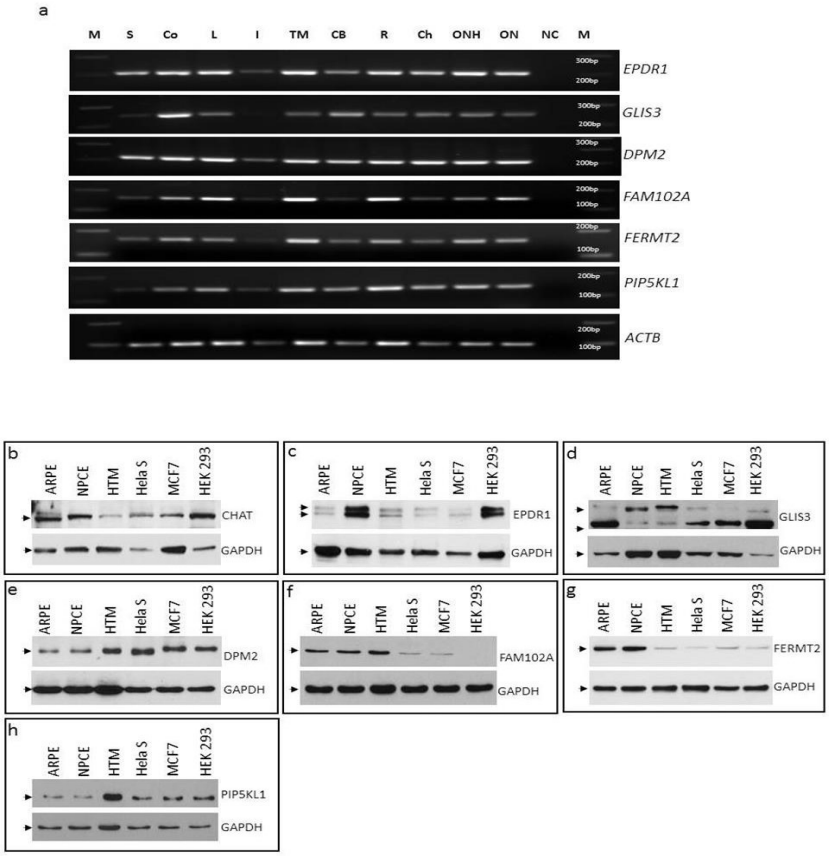

Ocular expression of genes at PACG-associated loci.

(**a**) Expression analysis of *EPDR1*, *GLIS3*, *DPM2*, *FAM102A*, *FERMT2*, and *PIP5KL1* in human ocular tissues by RT-PCR using genespecific primers (**Supplementary Table 9**). RT-PCR products were observed differentially in sclera (S), cornea (Co), lens with lens capsule (L), iris (I), trabecular meshwork (TM), ciliary body (CB), retina (R), choroid (Ch), optic nerve head (ONH), and optic nerve (ON). The ubiquitously expressed gene *ACTB* was used as the normalizing control. A no-template sample acted as the negative control (NC) to ensure no contamination of the RT-PCR reaction mix. M denotes the molecular weight marker. (**b**–**h**) Immunoblots of whole-cell lysates from retinal pigment epithelial (ARPE19), non-pigmented ciliary epithelial (NPCE), human trabecular meshwork (HTM), human cervical adenocarcinoma (Hela S), human breast adenocarcinoma (MCF7), and human embryonic kidney epithelial (HEK 293) cells, probed for CHAT, EPDR1, GLIS3, DPM2, FAM102A, FERMT2, and PIP5KL1 proteins and GAPDH, as a loading control. The protein isoforms detected by the respective antibodies were CHAT (83 kDa), EPDR1 (~25 kDa and ~18 kDa corresponding to two alternatively spliced forms of *EPDR1*), GLIS3 (~118 kDa and 90 kDa corresponding to two alternatively spliced forms of *GLIS3*), DPM2 (~17 kDa), FAM102A (37 kDa), FERMT2 (~78 kDa), and PIP5KL1 (22 kDa). The arrowheads indicate specific protein bands.

Supplementary Figure 3

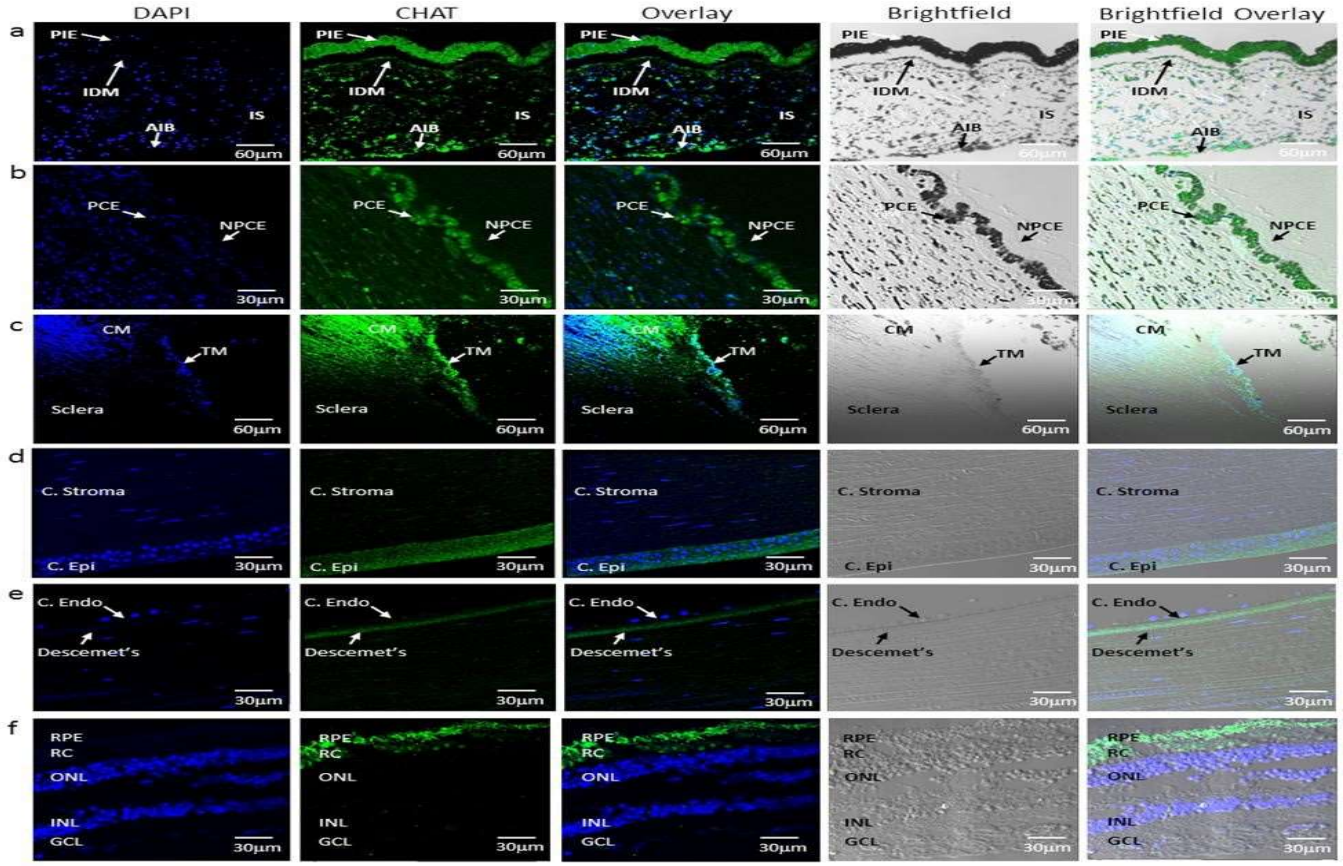

Analysis of CHAT distribution in human ocular tissues.

(**a**) Strong diffuse immunoreactivity of CHAT was detected in the posterior iris epithelium (PIE) and anterior iris border (AIB). In the iris stroma (IS), the iris stromal cells also show moderate to strong positive staining for CHAT, whereas the iris dilator muscle shows only weak and variable immunoreactivity. (**b**) In the ciliary body, pronounced yet diffuse staining of CHAT was detected in the pigmented ciliary epithelium (PCE). (**c**) The ciliary muscles (CM) showed strong and diffuse staining of the CHAT protein, whereas more moderate immunoreactivity was detected in the trabecular meshwork (TM) along the trabecular beams. (**d**,**e**) The corneal epithelium (C. Epi) and Descemet's membrane (Descemet's) demonstrated positive immunoreactivity for CHAT in contrast to the negative staining in stromal keratocytes, corneal stroma (C. Stroma), and endothelial cells (C. Endo). (**f**) In the retina, CHAT expression was diffusely and strongly positive in photoreceptors (PR). Negative immunoreactivity was seen in the nerve fiber layer, ganglion cell layer (GCL) inner plexiform layer, inner nuclear layer (INL), outer plexiform layer, and outer nuclear layer (ONL).

Supplementary Figure 4

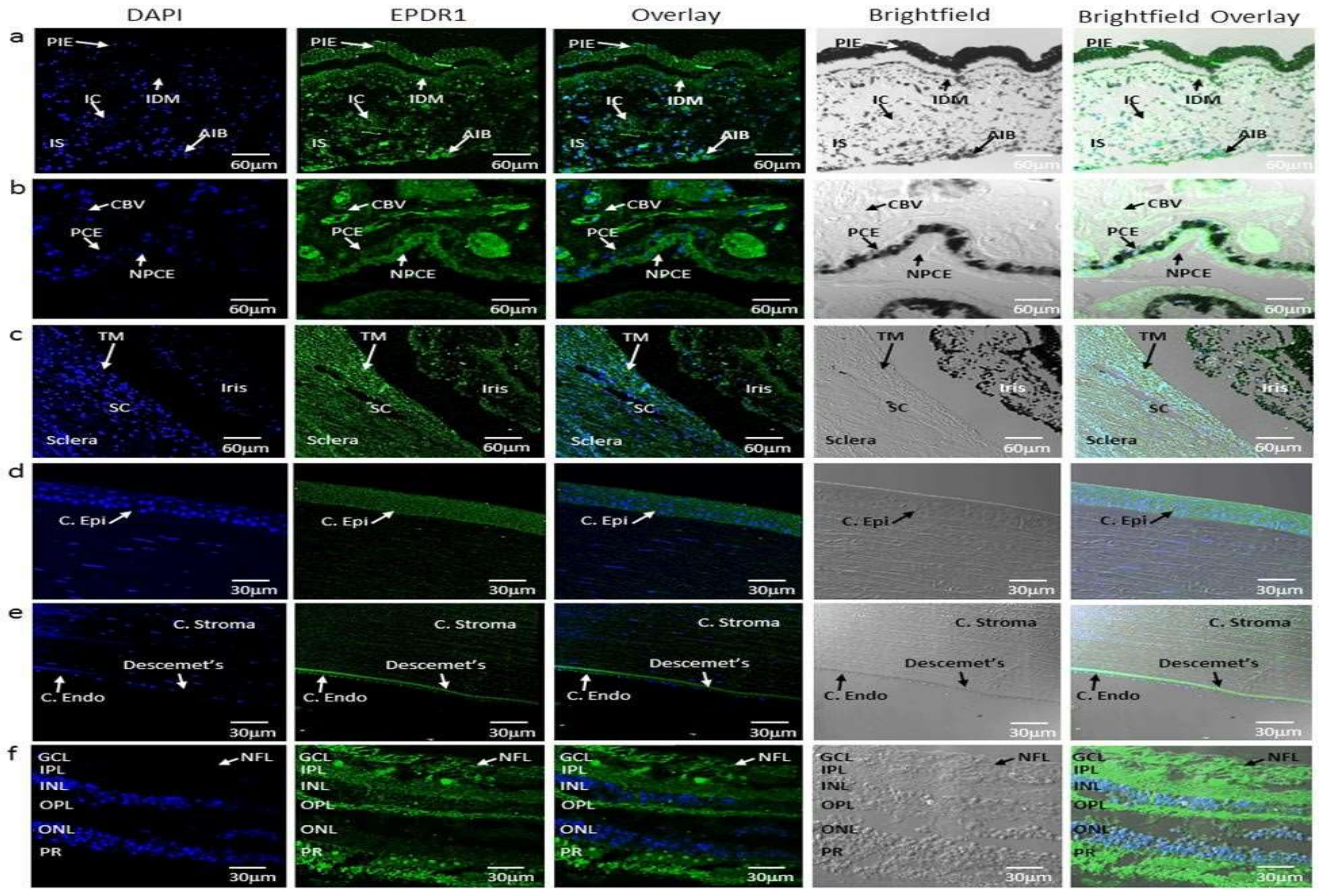

Analysis of EPDR1 distribution in human ocular tissues.

(**a**) In the iris, diffuse and strong immunoreactivity for EPDR1 was seen throughout the iris tissue. These areas included the posterior iris epithelium (PIE), iris dilator muscle (IDM), cells within the iris stroma (IS) as well as the iris capillaries (IC), and anterior iris border (AIB). (**b**) In the ciliary body, EPDR1 protein expression was detected as diffuse and strongly positive immunoreactivity in ciliary body vessels (CBV) and non-pigmented ciliary epithelium (NPCE). Although positive staining was detected in pigmented ciliary epithelium (PCE), the intensity was weaker than those for NPCE and CBV. (**c**) EPDR1 protein was also expressed throughout the trabecular meshwork (TM) and Schlemm's canal (SC). (**d**,**e**) In the cornea, EPDR1 was detected in the cornea epithelium (C. Epi.) and cornea endothelial (C. Endo) layers. (**f**) In the retina, EPDR1 staining was detected in the nerve fiber layer (NFL), ganglion cell layer (GCL), inner plexiform layer (IPL), outer plexiform layer (OPL), and photoreceptors (PR).

Supplementary Figure 5

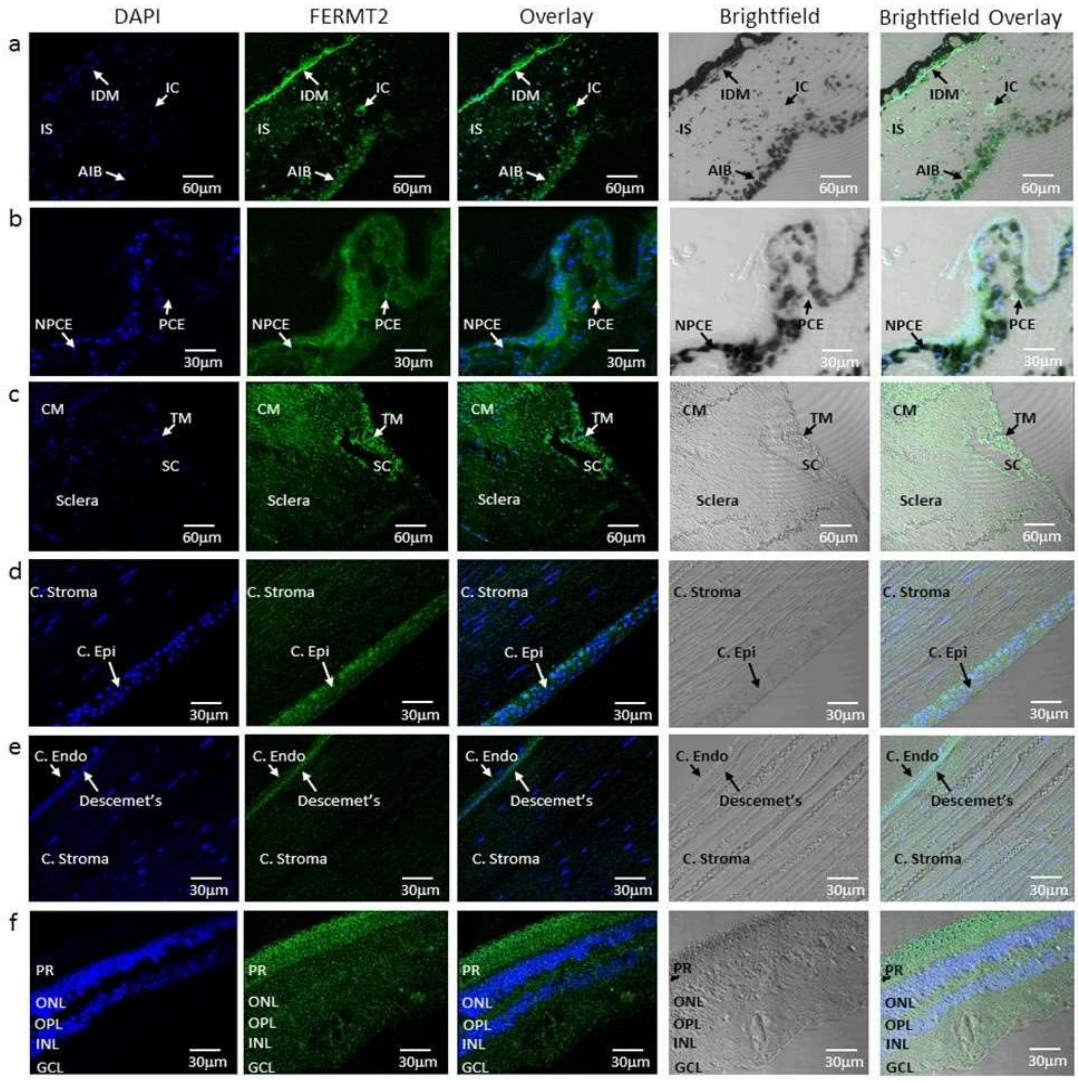

Analysis of FERMT2 distribution in human ocular tissues.

(**a**) In the iris, strong and diffuse FERMT2 immunoreactivity was detected in the iris dilator muscle (IDM). Moderate to strong immunoreactivity was also seen in cells within the iris stroma (IS) and iris capillaries (IC), whereas the anterior iris border showed only moderate immunoreactivity. (**b**) In the ciliary body, strong FERMT2 expression was detected in both non-pigmented ciliary epithelium (NPCE) and pigmented ciliary epithelium (PCE). (**c**) Strong FERMT2 immunoreactivity was detected in the ciliary muscles (CM), trabecular meshwork (TM), and Schlemm's canal (SC). (**d**,**e**) In the cornea, FERMT2 expression was observed in cornea epithelium (C. Epi.) and cornea endothelium (C. Endo.). (**f**) In the retina, FERMT2 was variably expressed in the retinal layers, with strong and diffuse immunoreactivity detected in the photoreceptors (PR) and moderate immunoreactivity seen in the outer plexiform layer (OPL).

Supplementary Figure 6

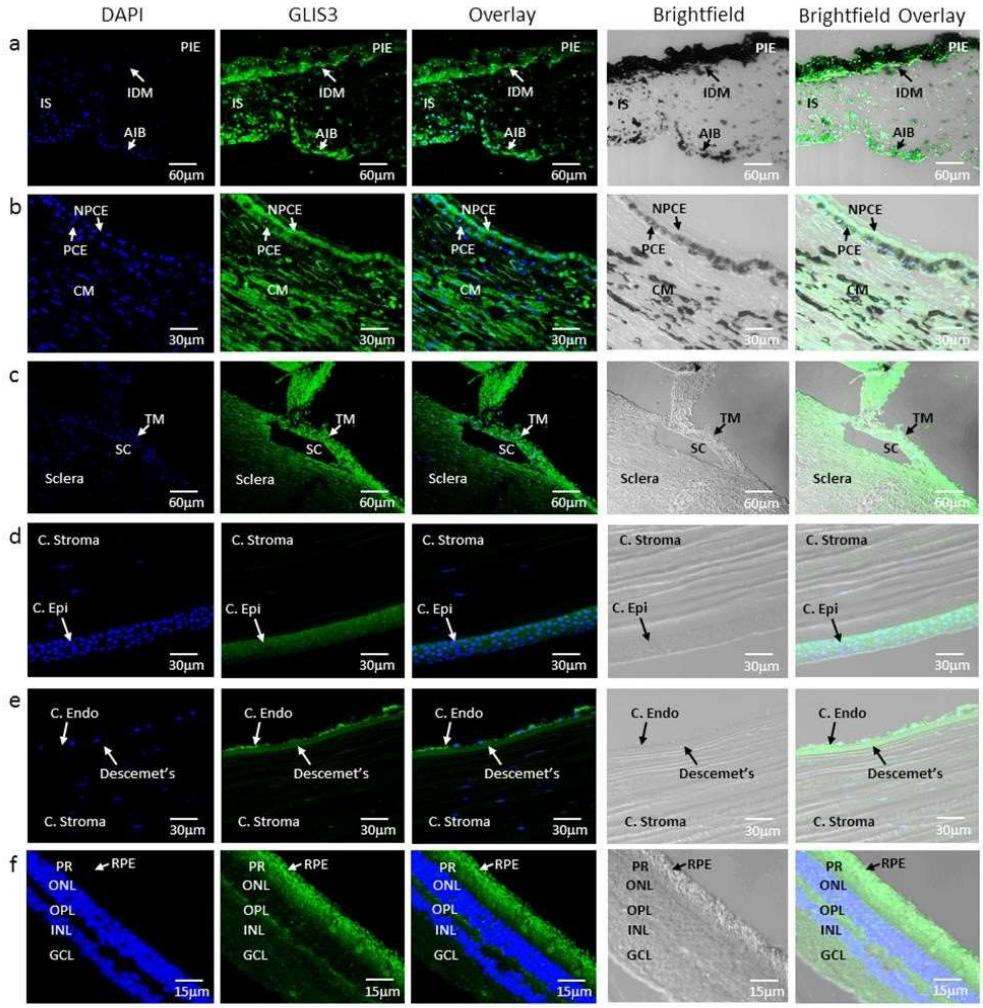

Analysis of GLIS3 distribution in human ocular tissues.

(**a**) In the iris, GLIS3 showed strong and diffuse immunoreactivity in iris dilator muscle (IDM) and the anterior iris border (AIB). A positive punctate membranous staining pattern in addition to weaker cytoplasmic staining was observed in posterior pigment epithelium of the posterior iris epithelium (PIE). The cells in the iris stroma (IS) also demonstrated strong positive GLIS3 immunoreactivity. (**b**) GLIS3 protein expression was prominently seen in the ciliary muscle (CM). Strong and diffuse immunoreactivity was detected in the nonpigmented ciliary epithelium (NPCE), pigmented ciliary epithelium (PCE), and ciliary muscle (CM). (**c**) In the trabecular meshwork (TM) and Schlemm's canal (SC), strong and diffuse immunoreactivity was detected. (**d**,**e**) In the cornea, GLIS3 expression was detected in the cornea epithelium (C. Epi.) and cornea endothelium (C. Endo.). (**f**) In the retina, distinct strong and diffuse GLIS3 immunoreactivity was detected in the photoreceptors (PR) and outer plexiform layer (OPL), with much weaker variable immunoreactivity detected in the ganglion cell layer (GCL).

Supplementary Figure 7

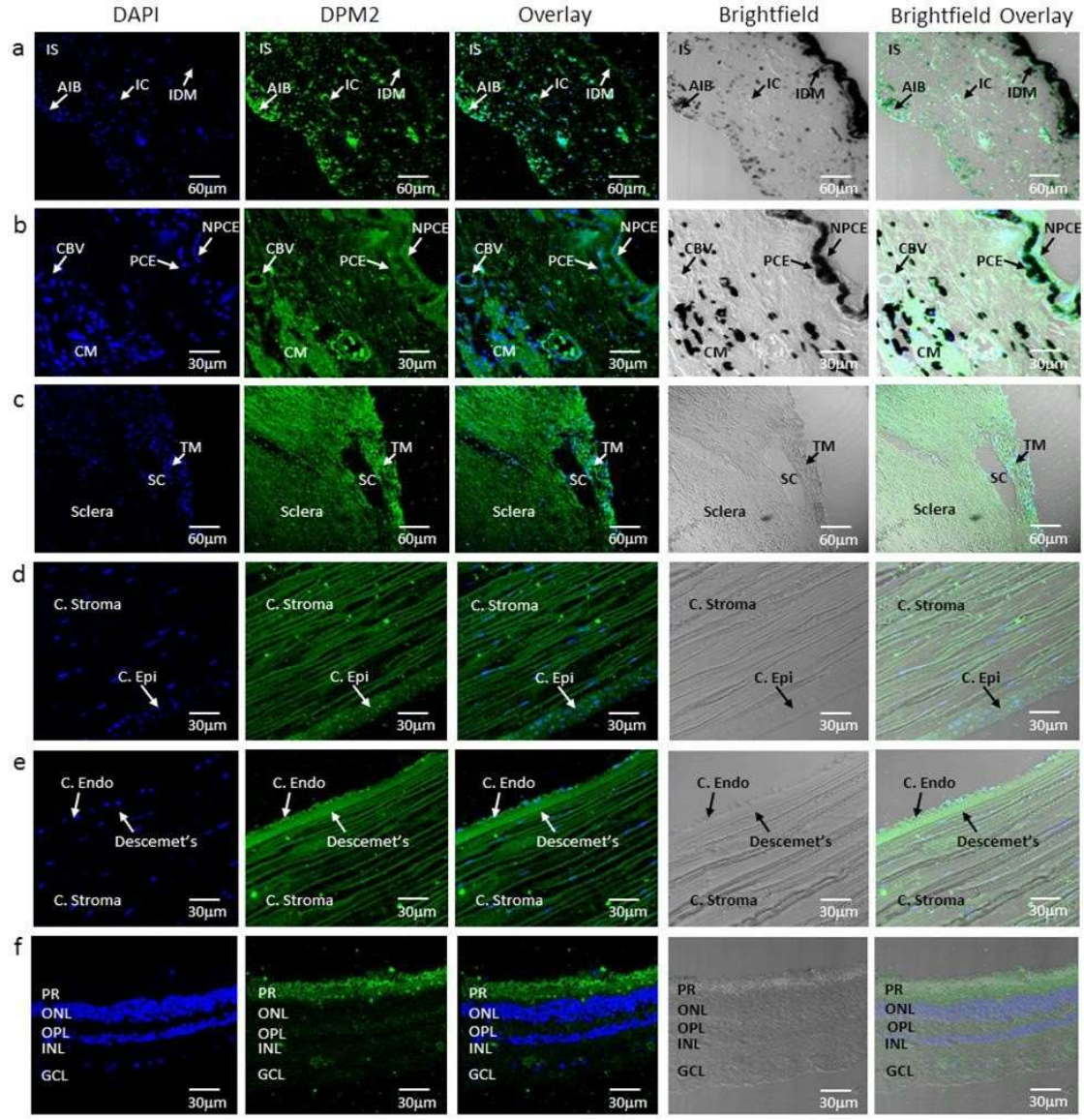

Analysis of DPM2 distribution in human ocular tissues.

(**a**) In the iris, strong DPM2 expression was detected in the anterior iris border (AIB), cells within the iris stroma (IS), and iris capillaries (IC), with only moderate intensity of DPM2 immunostaining detected in iris dilator muscle (IDM). (**b**) DPM2 protein was found to be diffusely expressed in the ciliary body. Strong immunoreactivity was detected in both non-pigmented ciliary epithelium (NPCE) and pigmented ciliary epithelium (PCE), ciliary body blood vessels (CBV), and also ciliary muscle (CM). (**c**) DPM2 immunoreactivity was seen in trabecular meshwork (TM) and Schlemm's canal (SC). (**d**,**e**) In the cornea, DPM2 expression was observed in cornea stromal (C. stroma) collagen fibers but not keratocytes. Immunoreactivity to DPM2 was also seen in the cornea epithelium (C. Epi) and cornea endothelium (C. Endo.). (**f**) In the retina, strong and diffuse immunoreactivity of DPM2 was detected in the photoreceptors (PR) in contrast to the much weaker immunoreactivity seen in the outer plexiform layer (OPL) and the ganglion cell layer (GCL).

Supplementary Figure 8

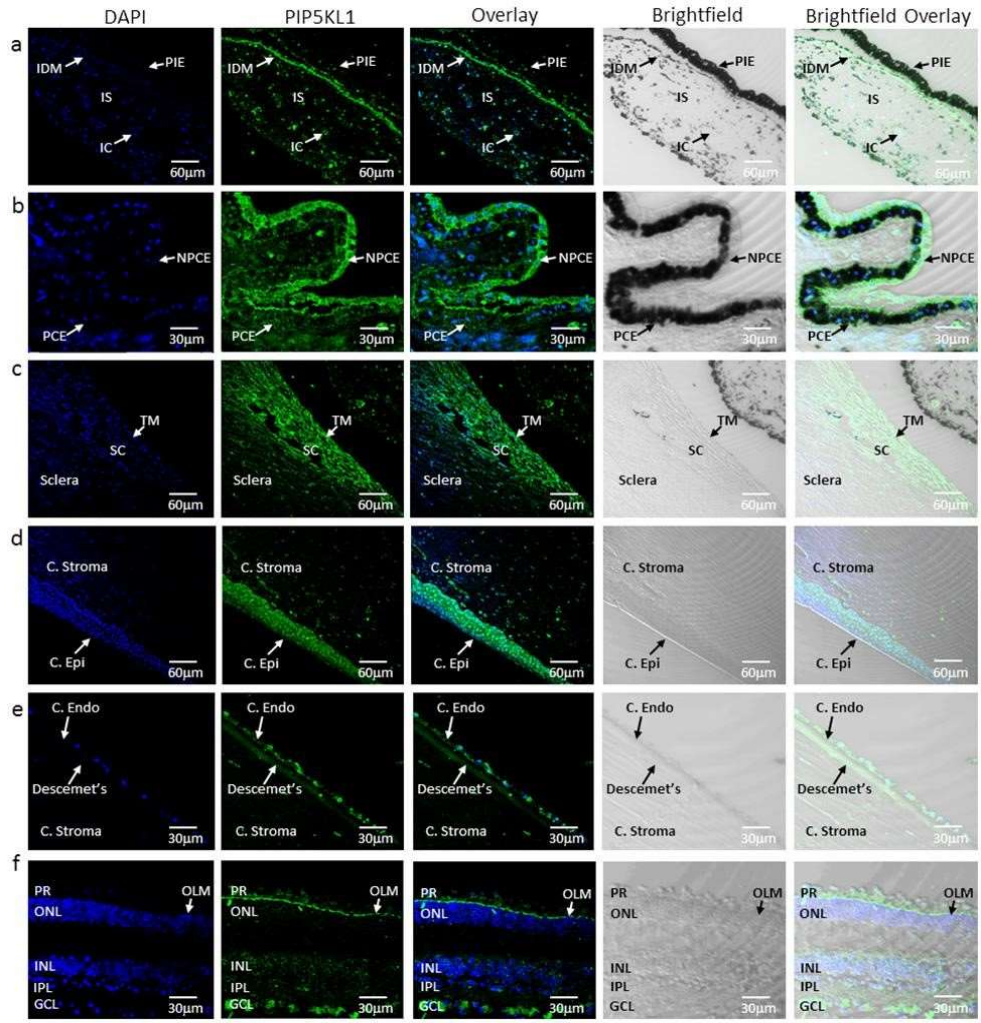

Analysis of PIP5KL1 distribution in human ocular tissues.

(**a**) In the iris, pronounced and diffuse staining of PIP5KL1 was detected in the iris dilator muscle (IDM). Strong immunoreactivity was also seen in iris stromal cells (IS) and iris capillaries (IC). (**b**) PIP5KL1 expression was diffuse with strong positive staining observed in the non-pigmented ciliary epithelium (NPCE). A weaker staining profile was observed in pigmented ciliary epithelium (PCE), which is constrained to PCE cell–cell borders. (**c**) In the trabecular meshwork (TM) and Schlemm's canal (SC), strong immunoreactivity of PIP5KL1 was detected in TM beams and endothelial cells of the Schlemm's canal. (**d**,**e**) In the cornea, PIP5KL1 was strongly expressed in the nuclei and cytoplasm of the corneal epithelium (C. Epi.). Positive staining of stromal keratocytes was also seen. The corneal endothelium (C. Endo) showed intense immunoreactivity to PIP5KL1. (**f**) In the retina, PIP5KL1 immunoreactivity in the outer limiting membrane (OLM) was distinctly prominent in comparison to the rest of the retinal layers. Similarly, the ganglion cell layer (GCL) also showed strong nuclear positive staining for PIP5KL1. In contrast, mild to moderate variable expression of PIP5KL1 protein was seen in photoreceptors (PR). Weak and variable immunoreactivity could be seen in the inner plexiform layer (IPL) and the inner nuclear layer (INL). The rest of the retina showed no significant immunoreactivity to PIP5KL1.

Supplementary Figure 9

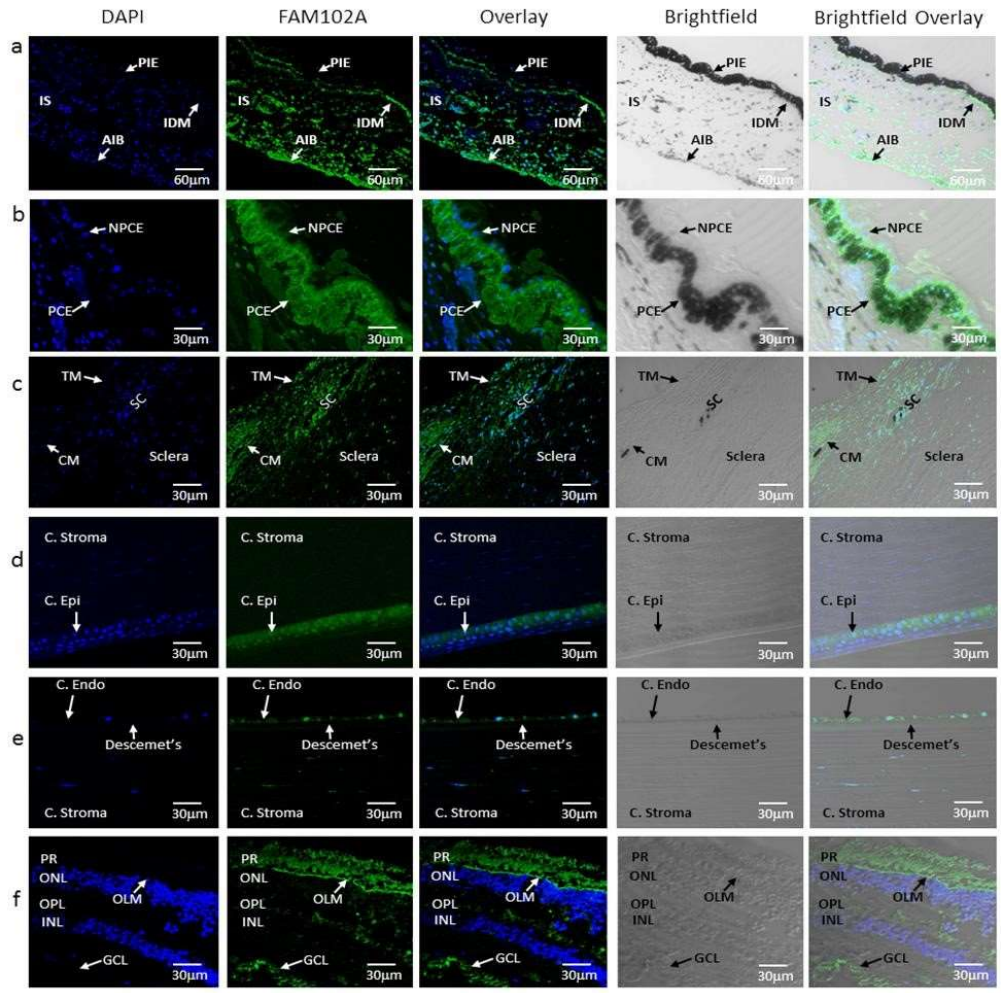

Analysis of FAM102A distribution in human ocular tissues.

(a) In the iris, strong immunoreactivity of FAM102A protein was seen in the anterior iris border (AIB), iris stromal cells (IS), and the iris dilator muscle (IDM). Moderate and punctate staining of the posterior border of the posterior pigment epithelium portion of the posterior iris epithelium (PIE) was also seen. (**b**) In the ciliary body, strong immunoreactivity for FAM102A protein was limited to pigmented ciliary epithelium (PCE) and non-pigmented ciliary epithelium (NPCE), with PCE having stronger immunoreactivity. (**c**) Moderate immunoreactivity of FAM102A was observed in the trabecular meshwork (TM), Schlemm's canal (SC), and ciliary muscle (CM). (**d**,**e**) In cornea, only the basal epithelial layer of the cornea epithelium (C. Epi.) and corneal endothelial cells (C. Endo.) showed moderate FAM102A protein immunoreactivity. (**f**) In the retina, strong FAM102A immunoreactivity was distinctly localized to the outer limiting membrane (OLM), photoreceptors (PR), and nuclei of the ganglion cell layer (GCL). Patchy moderate immunoreactivity of FAM102A was also noted in the outer plexiform layer (OPL). The rest of the retinal layers showed no significant immunoreactivity to FAM102A.

Supplementary Figure 10

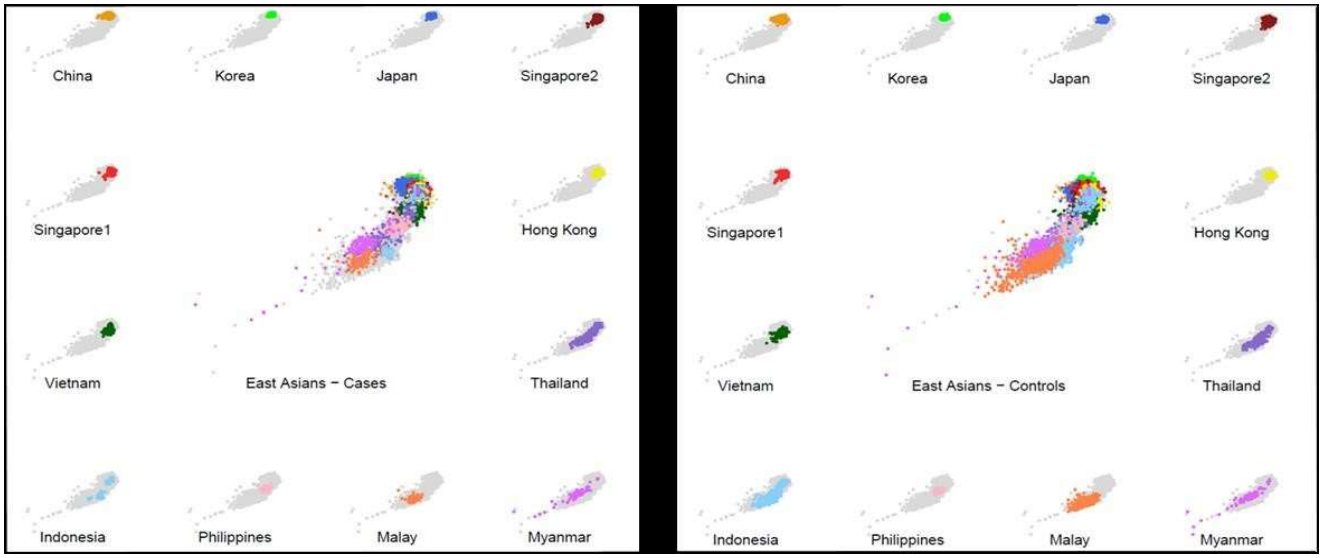

Distribution of PACG cases and controls of East Asian descent from the GWAS discovery stage.

PACG cases and controls are projected onto the top two principal components of genetic stratification, with cases on the left panel and controls on the right panel.

Supplementary Figure 11

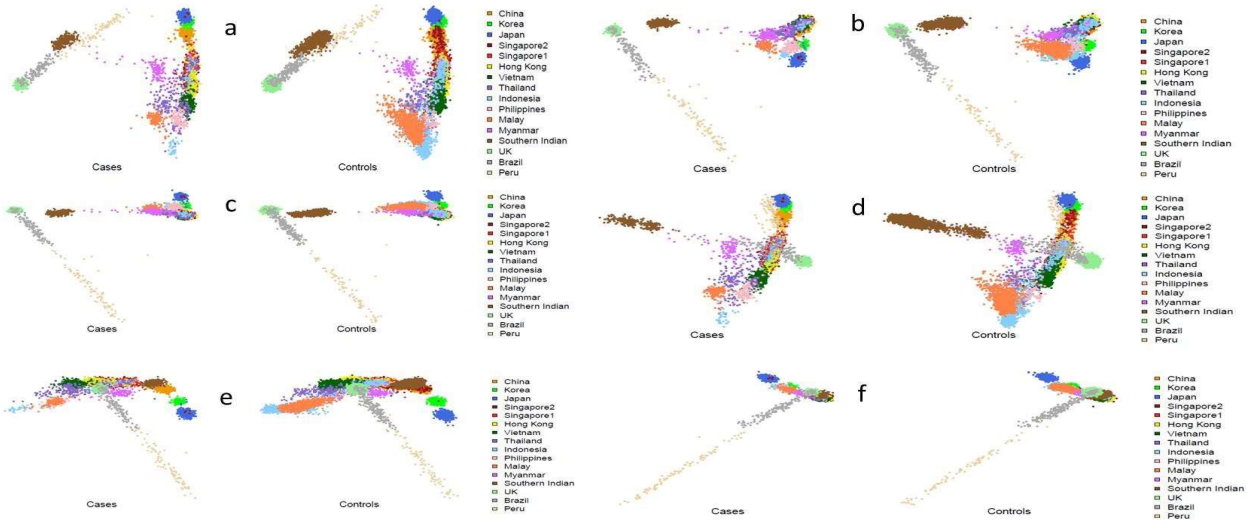

Detailed ancestry analysis of PACG cases and controls from the GWAS discovery stage, which encompassed collections from 15 countries.

(**a-f**) The genetic principal components (PCs) for cases and controls are projected onto PC1 vs. PC3 (**a**), PC1 vs. PC4 (**b**), PC1 vs. PC5 (**c**), PC2 vs. PC3 (**d**), PC3 vs. PC4 (**e**), and PC4 vs PC5 (**f**). For each panel, PACG cases are projected on the left and controls on the right.

Supplementary Figure 12

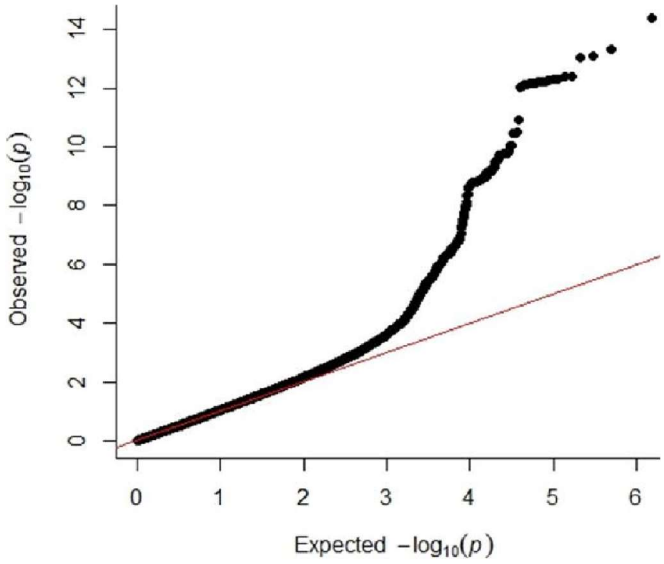

Quantile-quantile plot showing the association results for the GWAS discovery stage encompassing 6,525 PACG cases and 19,929 controls.

Supplementary information

Supplementary Note

Details for PACG case control collections.

Inclusion Criteria

1. Patients with acute primary angle closure (APAC) or primary angle closure glaucoma (PACG) were recruited 2. Informed consent
3. Age more than 21 years

Definition for Acute Primary angle-closure (APAC)

Previous APAC was defined as the presence of at least two of the following symptoms: ocular or periocular pain, nausea or vomiting or both, and an antecedent history of intermittent blurring of vision; a presenting IOP of more than 28 mmHg on Goldmann applanation tonometry; and the presence of at least three of the following signs: conjunctival injection, corneal epithelial edema, mid-dilated non-reactive pupil, and shallow anterior chamber.

Definition for Primary angle-closure glaucoma (PACG)

Defined for cases of gonioscopic angle-closure (at least 180 degrees of angle closure in which the trabecular meshwork was not visible on gonioscopy) with glaucomatous optic neuropathy. This is defined as disc excavation with loss of neuroretinal rim tissue and a vertical cup: disc ratio greater than the 97.5 percentile of the population (0.7), when examined with a 78D biomicroscopic lens. In addition, for PACG diagnosis, there was the presence of visual field loss detected with static automated white-on-white threshold perimetry (program 24-2 SITA, model 750, Humphrey Instruments, Dublin, Ca) that is consistent with glaucomatous optic nerve damage. This is defined as Glaucoma Hemifield test outside normal limits and/or an abnormal pattern standard deviation with $P<5\%$ occurring in the normal population.

Approximately 40% of patients in this study had APAC whilst the remaining patients had PACG.

The unifying characteristic of all these patients is that the cause of their angle closure is not secondary to any other pathology (hence classified as primary) and that all patients have gonioscopic angle closure with significant disease severity.

Distinction between APAC and PACG

Approximately 40% of patients in this study had APAC whilst the remaining patients had existing PACG.

The unifying characteristic of all these patients is that the cause of their angle closure is not secondary to any other pathology (hence classified as primary) and that all patients have gonioscopic angle closure with significant disease severity.

The clinical classification of APAC and PACG, which is based on reported symptoms in patients, is rather anachronistic. Such a distinction is subjective and likely to be affected by recall bias. Further scenarios may blur the distinctions; patients with existing PACG may have had intermittent angle closure or subclinical

episodes before; acute attacks may occur on a background of existing PACG, and patients with APAC may proceed to develop chronic ACG as a result of persistently raised intraocular pressure (IOP).

The International Society of Geographical and Epidemiological Ophthalmology (ISGEO)
[1] recommended a revised approach to classification of ACG which does not include symptoms,
i.e. does not differentiate between APAC and existing PACG. This approach was supported by a subsequent report which reported a high rate of symptoms traditionally associated with APAC in an unaffected normal population[2]. The ISGEO approach to classification is now the standard approach to classification of angle closure glaucoma, and centers on the concept that:

- Primary angle-closure disease is contact between iris and trabecular meshwork outflow channels occurring in the absence of any other ocular pathology
- This contact is sufficient to significantly obstruct aqueous fluid outflow, causing elevated IOP
- Symptoms are a poor indicator of the presence or absence of disease, and unrelated to the natural history of the disease
- The only relevance of symptomatic characteristics is that acute attacks (being painful and associated with transient, visual disturbance) are more likely to lead to earlier presentation.

We therefore feel that grouping APAC and PACG cases together in this analysis is entirely reasonable as the thrust of our analysis is to study the molecular biology of development of PACG. The current understanding of this disease and its management does not support any scientific basis for separation of acute and chronic presentations.

Controls

1. Patients with no evidence of glaucoma or major ocular disease such as diabetic retinopathy, age related macular degeneration or conditions with genetic background will be considered as controls.
2. Age more than 40 years
3. Informed consent

GWAS discovery collections

Patients with PACG and controls were drawn from 15 countries and considered within 16 distinct strata for analysis (**Supplementary Table 1**).

Singapore: Cases of PACG included patients with chronic PACG or those with APAC (as defined above). All Singapore PACG cases for the GWAS discovery stage were recruited between years 2005 – 2015 from Singapore National Eye Centre, Tan Tock Seng Hospital, National University Hospital and Changi General Hospital. Controls were ascertained from an on-going population based study of Chinese persons aged 40 years and older (the Singapore Chinese Eye Study [SCES]). The SCES is a population-based, cross-sectional study of Chinese adults residing in the south- western part of Singapore. The Ministry of Home Affairs of Singapore provided an initial computer-generated list ethnic Chinese names of adults aged 40-80+ years of age. A final sampling frame of 6,350 ethnic Chinese residents was derived from this list using an agestratified random sampling strategy. A control was defined as IOP < 21 mm Hg with open angles, healthy optic nerves and normal visual fields, and no previous intraocular surgery. Ethics approval was obtained from the respective institutional review boards (IRBs).

Beijing: PACG patients were recruited from the Beijing Tongren Hospital, Xingtai Eye Hospital and Anyang Eye Hospital, China. The diagnostic criteria for PACG were as described above. Controls were recruited from the Handan Eye Study (HES), a population-based study of eye disease in rural Chinese aged 40 years and over. The criteria for selecting controls are also as described above.

Hong Kong: Patients with PACG were defined as above. All subjects of the Hong Kong study population were recruited from the Prince of Wales Hospital, Queen Mary Hospital, University of Hong Kong, and the Hong Kong Eye Hospital, Hong Kong under the approval from the Ethics
Committee on Human Research of the Chinese University of Hong Kong and University of Hong Kong. A total of 303 PACG patients of Han Chinese ancestry were recruited. The controls comprised of 225 Hong Kong Chinese and 976 Guangdong Chinese of Han ancestry, of which 1,049 were genotyped (73 from Hong Kong and 976 from Guangdong) and 1,044 passed quality checks (73 Hong Kong and 971 from Guangdong). The Hong Kong control subjects were recruited in a hospital-based manner. They were all given complete ocular examinations, and confirmed to have no sign of glaucoma, angle closure or narrow angle, or other major eye diseases except for mild cataract and mild refractive errors. Control subjects were recruited from elderly people aged ≥ 60 years to ensure they were at least free of early-onset major eye diseases. They had IOP < 21 mmHg, and had no known family history of glaucoma. Additional healthy controls were recruited from local communities in the Guangdong province of Southern China[3].

Vietnam: PACG cases were defined as above. They were recruited from the Vietnam National Institute of Ophthalmology in Hanoi, from the Hue University of Medicine and Pharmacy in Danang City, from Viet Tiep General Hospital in Hai Phong, as well as Ho Chi Minh City Eye Hospital in Ho Chi Minh City, Vietnam. The hospital Institutional Review Boards approved the study from each site. The controls comprise 2,018 cord bloods from the general population, as previously described[4,5].

Malaysia: PACG was defined using the same criteria as above. The PACG cases were recruited from the:

1. Department of Ophthalmology, School of Medical Sciences, Universiti Sains Malaysia, Kota Bharu, Kelantan, Malaysia, as previously described[6]
2. International Specialist Eye Centre, Kuala Lumpur. The International Specialist Eye Center Ethics Committee approved the study.
3. Department of Ophthalmology, Hospital Kuala Lumpur, Kuala Lumpur, Malaysia. The study was approved by the Medical Research and Ethics Committee of the Ministry of Health Malaysia.
4. Department of Ophthalmology, Universiti Malaya, Kuala Lumpur.

Ethics approval was obtained from the respective IRBs. The controls were a population-based collection of healthy ethnic Malays recruited from Singapore (N = 3065), as previously described[6]. A total of 1119 controls were well-matched ancestrally to the PACG cases and were included for association analysis.

India: PACG cases (as defined above) of South Indian ancestry were recruited from a large population based cross sectional study, the Chennai Glaucoma study, and from the outpatient department of the Medical Research Foundation, Sankara Nethralaya, Chennai, India. All PACG cases had peripheral anterior synechiae on gonioscopy, and were identified prior to laser iridotomy. The Chennai Glaucoma study recruited 7851 persons from rural and urban cohorts in the Southern Indian state of Tamil Nadu. The controls were a population-based collection of healthy ethnic Indians recruited from Singapore (N = 2538), as previously described[6].

United Kingdom: Cases of PACG in the UK were defined using the same criteria as defined above. All subjects were of UK European descent and were recruited from Moorfields Eye Hospital, London; the Oxford Eye Hospital, John Radcliffe Hospital, Oxford University Hospitals
NHS Foundation Trust (sample collection sponsored by University College London); the
Department of Ophthalmology, University of Nottingham, as well as the BMI Park Hospital Nottingham. This study was approved by the Nottingham Research and Ethics Committee and the East Central London Research and Ethics Committee. The controls comprised of 4,703 healthy individuals of UK European descent, recruited and genotyped by the Wellcome Trust Case-Control Consortium 2. Their extensive use for genetics studies (such as ankylosing spondylitis, psoriasis, ulcerative colitis, ischaemic stroke, Meningococcal sepsis, and Kawasaki disease) has been well-described[7-11].

Japan: Cases of PACG in Japan were defined using the same criteria as defined above. All subjects were of Japanese descent and were recruited from the Department of Ophthalmology,
Kobe City Medical Center General Hospital; Ozaki Eye Hospital in Hyuga; Oita University
Hospital, Medical Foundation Tenshindo, Oita Prefectural Hospital, National Hospital Organization Beppu Medical Center, Shin Beppu Hospital, Mizoguchi Eye Hospital in Nagasaki, as well as from the University Hospital of the Kyoto Prefectural University of Medicine, Baptist Eye Clinic, and Oike Ikeda Eye Clinic (all in Kyoto city). Research protocols were approved by the institutional review boards of the Kobe City Medical Center General Hospital, the IRB committee of Ozaki Eye Hospital (which includes faculty members from the Kyushu University of Health and Welfare), Mizoguchi Eye Hospital, the Ethics Committee of Oita University Faculty of Medicine, as well as the Institutional Review Board of the Kyoto Prefectural University of Medicine. The controls were individuals aged 60 years and above without any eye diseases enrolled in neighboring eye hospitals, as previously described[12].

Korea: Cases of PACG were defined using the same criteria as defined above. All PACG cases and controls were obtained from the subjects seen at the glaucoma clinic of Severance Hospital at Yonsei University College of Medicine; Kim's Eye Hospital, Seoul, as well as the Department of Ophthalmology, Seoul National University Hospital, Seoul National University College of Medicine, Seoul, South Korea. The Institutional Review Board of the Yonsei University Health
System approved the study protocol. The study protocol was also approved by the Institutional
Review Board at Kim's Eye Hospital, Seoul, Korea as well as by the Seoul National University Hospital Institutional Review Board. All procedures conformed to the guidelines of the Declaration of Helsinki and informed consent was obtained from the patients.

Brazil: PACG cases and controls were defined using the same criteria as defined above. They were recruited at the University of Campinas Clinical Hospital. Ethical approval was granted by the University of Campinas Clinical Hospital, Sao Polo, Brazil as Certificate of Presentation for Ethical Appreciaction (Certificado de Apresentação para Apreciação Ética or CAAE):
14722313.2.0000.5404 to Dr Monica Melo.

Indonesia: PACG cases were defined using the same criteria as defined above. The PACG cases were recruited at the Jakarta Eye Center, Indonesia. The Jakarta Eye Center Ethics Committee approved the study. The controls used in the Indonesian cohort were subjects recruited in a hepatitis B vaccine efficacy trial. The participants of this trial were residing on Batam and surrounding islands in the Indonesia's Riau Archipelago. A two-dose vaccination schedule (Engerix-B, 20µg/L recombinant HBsAg; GlaxoSmithKline Biologicals, Belgium) was completed in 13,315 subjects, who were over 5 years of age. Subjects who were anti-HBc, anti-HBs or HBsAg positive at entry (N = 4,802; 25%) were excluded. Post vaccination antibody titer was measured (Elecsys system, Boehringer/Roche, Germany) 6 months after the final dose in about 5,100 subjects from whom DNA was available, forming the study base for the genetic association study[13].

Myanmar: PACG cases and controls were defined using the same criteria as defined above. The PACG cases and controls were recruited from Defence Services General Hospital, Myanmar Eye Centre, Pun Hlaing Siloam Hospital; Shwe La Min Hospital, as well as the Mandalay Eye department, Mandalay Eye ENT hospital, University of Medicine Mandalay. The Hospital General Management committees approved the study. Final ethical approval was obtained from the Myanmar Ministry of Health.

Peru: PACG patients and controls were defined using the same criteria as defined above. They were recruited from the Instituto de Glaucoma y Catarata, Lima, Perú. Ethical approval for the study was granted by the Comité Institutional de Etica en Investigación de la Universidad de San Martín de Porres-Clínica Cada Mujer, Lima, Perú (IRB00003251-FWA0015320).

Philippines: PACG cases and controls were defined using the same criteria as defined above, and recruited at the Pasig City General Hospital, Metro Manila and the Asian Eye Institute at Makati City. The study protocol was reviewed and approved by the Pasig City General Hospital Ethics Review Board and the Ethics Review Committee of the Asian Eye Institute.

Thailand: PACG cases were defined using the same criteria as defined above. The PACG cases were enrolled at Department of Ophthalmology, Faculty of Medicine Siriraj Hospital, Mahidol University, Bangkok, Thailand, at the Glaucoma Service, Department of Ophthalmology, Rajavithi Hospital, Bangkok, Thailand, at Department of Ophthalmology, Thammasat University Faculty of Medicine, Rangsit, Thailand, at Department of Ophthalmology, Faculty of Medicine, Chiang Mai University, Chiang Mai, Thailand, and at Department of Ophthalmology, Faculty of Medicine, Chulalongkorn University, Bangkok, Thailand. Ethical approval was granted by the Ethics committee, Rajavithi hospital, Bangkok, by the Human Ethics Committee of Thammasat University, by the Siriraj Institutional Review Board, Faculty of Medicine Siriraj Hospital, by the Institutional Review Board, Faculty of Medicine, Chulalongkorn University, Bangkok, Thailand, and by the Chiang Mai University Hospital in Chiang Mai, Thailand. The non-PACG controls from Thailand have been previously described[14].

Replication collections

Saudi Arabia: PACG cases and controls were defined as above. They were collected at the glaucoma clinic at the King Abdulaziz University Hospital, Department of Ophthalmology, College of Medicine, King Saud University as well as at the King Khaled Eye Specialist Hospital (both in Riyadh), Saudi Arabia. All patients and controls were unrelated Saudi Arabs, all whose known ancestors were of Saudi Arabian origin. As judged by the family names, PACG patients and controls were representative of the five provinces of the Kingdom of Saudi Arabia. The study was approved by College of Medicine IRB committee, King Saud University, and the IRB of the King Khaled Eye Specialist Hospital, Riyadh, Saudi Arabia. All participants signed an informed consent.

Australia: The PACG case and control groups were defined using the same criteria as defined above. Participants were recruited from Ophthalmology clinics in Australia. Ethical approval was obtained from the human research ethics committees of the Southern Adelaide Health Service/Flinders University, and the study was conducted in accordance with the Declaration of Helsinki and its subsequent revisions. Informed written consent was obtained from each individual. The Australian cohort is of self-reported Caucasian ethnicity. The Australian control cohort was obtained from the Blue Mountain Eye Study, as previously described[12,15,16].

Mexico: The PACG case and control groups were defined using the same criteria as defined above. Participants are recruited from the Department of Glaucoma, Institute of

Ophthalmology "Conde de Valenciana", Mexico City, Mexico. Written informed consent was obtained from all participants, the study protocol was approved by the Hospital ethics committee, and the study was performed according to the tenets of the Declaration of Helsinki.

Nepal: The PACG cases were defined using the same criteria as defined above. Participants were recruited from Ophthalmology clinics in Nepal. Ethical approval was obtained from Nepal Glaucoma Eye Clinic, Tilganga Institute of Ophthalmology, Kathmandu Nepal, and the study was conducted in accordance with the Declaration of Helsinki and its subsequent revisions. Informed consent was obtained from each individual. The Nepalese control group was enrolled from Patan Hospital in Kathmandu, Nepal, as previously described[4]. Individuals were chosen specifically to be matched for age, gender and ethnic group to the Nepalese cases.

Okinawa: PACG cases and controls were defined as above. Ethical approval was granted by the University of the Ryukyus Institutional Review Board.

Poland: PACG cases and controls were defined as above. APAC, PACG and control patients were recruited from the Department of Diagnostics and Microsurgery of Glaucoma, Medical University, Lublin, Poland. All patients self-reported as Caucasians. The informed consent was obtained before the enrollment, the protocol was approved by local ethical committee in Medical University of Lublin (approval number 174/14). All patients from the studied group had documented acute primary angle closure. Patients diagnosed with secondary angle closure were excluded. Patients from the control group had performed surgery because of simple cataract, patients with any type of glaucoma, ocular hypertension or any other ocular disease except from cataract were excluded.

Beijing: PACG patients and controls were defined as above, and were recruited in a similar manner to those samples enrolled for the GWAS discovery stage.

Hong Kong: PACG patients and controls were defined as above, and were recruited in a similar manner to those samples enrolled for the GWAS discovery stage.

Singapore: PACG patients and controls were defined as above, and were recruited in a similar manner to those samples enrolled for the GWAS discovery stage.

Vietnam: PACG patients and controls were defined as above, and were recruited in a similar manner to those samples enrolled for the GWAS discovery stage.

North India: PACG patients and controls were defined as above. PACG cases of North Indian ancestry were recruited from the Glaucoma Clinic and the Outpatient Department of Dr.
Rajendra Prasad Centre for Ophthalmic Sciences, All India Institute of Medical Sciences, New Delhi, India. All PACG cases had peripheral anterior synechiae on gonioscopy and were identified prior to laser iridotomy. The controls were healthy ethnic North Indians recruited in a hospital-based manner. They were all given complete ocular examinations and confirmed to have no sign of glaucoma, angle closure or narrow angle or other major eye diseases. This study was approved by the Institute Ethics Committee of All India Institute of Medical Sciences, New Delhi, India.

South India: PACG patients and controls were defined as above, and were recruited in a similar manner to those samples enrolled for the GWAS discovery stage. PACG cases of South Indian ancestry were recruited from the glaucoma clinics of Narayana Nethralaya Eye Hospital in Bangalore and Aravind Eye Hospital in Tamilnadu, India. Ethical approval was granted by the Narayana Nethralaya Hospital Ethics Committee. The Institutional Review Board of the Aravind Eye care System also reviewed and approved the project.

Pakistan: PACG patients and controls were defined as above. All the samples of angle closure had primary glaucoma and included patients of chronic and acute PACG whereas the controls had no such signs and symptoms and no positive findings in history and examination. All the patients as well as the controls were of Pakistani origin, belonging mostly to the northern provinces of Pakistan including; Punjab and Khyber Pakhtunkhwa. The patients were recruited from Al-Shifa Eye Trust Hospital (Pakistan Institute of Ophthalmology), Rawalpindi, Pakistan, after obtaining their informed written consent. The work was approved by the Ethics Review Board of the Department of Biosciences, COMSATS Institute of Information Technology, Islamabad, Pakistan and adhered to the tenets of the Helsinki Declaration.

Italy: PACG patients and controls were defined as above. PACG cases were enrolled at the Dipartimento di Scienze Chirurgiche – Universita' di Torino, Torino, Italy. All patients and controls were unrelated Italians, all whose known ancestors were of Italian origin. The Comitato Etico Interaziendale A.O.U. San Giovanni Battista di Torino approved the study.

USA: PACG patients and controls were defined as above. Patients with PACG were enrolled from the New York Eye and Ear Infirmary, New York University. The controls were enrolled from the New York Eye and Ear Infirmary as well as University of Iowa. The study was approved by the IRB of the New York Eye and Ear Infirmary of Mount Sinai, New York, NY. All participants from Iowa provided informed consent and the study were approved by the University of Iowa's IRB Board.

Supplementary Table 1

a) Summary of GWAS discovery case-control collections. The number of principal components adjusted for, as well as the genomic inflation factor for each collection was included. GWAS1 refers to PACG case-control collections previously described in Vithana E et al., *Nat Genet* 2012; 44:1142-1146. GWAS2 refers to current freshly genotyped samples.

	N	N	Number of principal	
Discovery collection name	PACG cases	controls	components adjusted for	λgc
Hong Kong GWAS1	297	1044	PC1-PC3	1.012
India GWAS1	337	2538	PC1-PC10	1.067
Singapore GWAS1	984	943	None	1.022
Vietnam GWAS1 + GWAS2	1423	2018	PC1-PC5	1.058
Malays GWAS1 + GWAS2	147	1119	PC1-PC15	1.076
Japan GWAS2	422	952	PC1-PC3	1.0056
Korea GWAS2	118	541	PC1-PC3	1.0026
Singapore GWAS2	1077	2641	PC1-PC3	1.029
China GWAS2	623	1111	PC1-PC5	1.00
Brazil GWAS2	136	203	None	1.00
Indonesia GWAS2	66	1609	PC1-PC3	1.0069
Myanmar GWAS2	138	143	None	1.00
Peru GWAS2	85	82	None	1.00
Philippines GWAS2	78	58	PC1	1.00
Thailand GWAS2	239	272	PC1	1.02
UK GWAS2	355	4655	PC1-PC3	1.022
	6525	**19929**		**5**
Total GWAS				1.0

b) Summary of the replication case-control collections.

Replication collection name	N PACG cases	N controls
Australia	150	2574
Nepal	90	205
Okinawa	234	324
Poland	144	165
Beijing	1557	1793
Hong Kong	65	981
Singapore	271	303
Vietnam	213	464
North India	100	93
South India	259	287
Pakistan	269	172
Saudi Arabia	391	1659
Italy	72	223
Mexico	99	224
USA	64	171
Total replication	**3978**	**9638**
Total discovery & replication	**10503**	**29567**

Supplementary Table 2

Summary of the discovery and replication results for 10 sentinel SNPs representing the 10 independent loci surpassing $P < 1 \times 10^{-6}$ in the GWAS discovery stage.

						Discovery		Replication	
Chr	**Position**	**Locus**	**SNP-id**	**Effect allele**	**Reference allele**	**OR**	***P*-value**	**OR**	***P*-value**
1	103379918	*COL11A1*	rs3753841	G	A	1.18	1.18×10^{-11}	1.29	1.15×10^{-14}
3	171794511	*FNDC3B*	rs16856870	A	G	0.76	1.65×10^{-10}	1.00	0.92
7	37988311	*EPDR1*	rs3816415	A	G	1.28	1.28×10^{-12}	1.17	0.00032
8	52887541	*PCMTD1-ST18*	rs1015213	A	G	1.44	1.75×10^{-9}	1.40	5.47×10^{-8}
9	4217028	*GLIS3*	rs736893	G	A	1.16	4.23×10^{-8}	1.20	4.64×10^{-8}
9	130702477	*DPM2-FAM102A*	rs3739821	G	A	1.17	7.08×10^{-10}	1.11	0.0013
10	50895770	*CHAT*	rs1258267	A	G	1.25	5.06×10^{-14}	1.16	0.00046
11	17008605	*PLEKHA7*	rs11024102	G	A	1.2	4.1×10^{-15}	1.15	5.51×10^{-5}
14	53411391	*FERMT2*	rs7494379	G	A	1.15	9.26×10^{-9}	1.11	0.00065
14	61511165	*SLC38A6*	rs10483730	A	G	0.86	1×10^{-6}	0.95	0.18

Supplementary Table 3

Association results for the three previously reported PACG loci in this study, as well as excluding previously reported samples from Vithana E et al. 2012[6].

					This study		**Excluding previously reported samples[6]**	
Gene	**Chromosome**	**Position**	**SNP**	**Risk allele**	**OR**	***P***	**OR**	***P***
PLEKHA7	11	17008605	rs11024102	G	1.18	1.93×10^{-18}	1.17	9.56×10^{-10}
COL11A1	1	103379918	rs3753841	G	1.21	1.27×10^{-23}	1.23	1×10^{-14}
PCMTD1-ST18	8	52887541	rs1015213	A	1.42	$5.42. \times 10^{-16}$	1.45	5.98×10^{-9}

Supplementary Table 4

Statistical power calculations as a function of minor allele frequency (MAF) and allele odds ratio for a) the discovery GWAS stage with 6,525 PACG cases and 19,929 controls at $P < 1 \times 10^{-6}$ and b) the combined discovery and replication meta-analysis comprising 10,503 PACG cases and 29,567 controls at $P < 5 \times 10^{-8}$. Conditions fulfilling ≥80 percent statistical power are highlighted in yellow. a)

Odds Ratio

MAF	1.10	1.15	1.20	1.25	1.30	1.35	1.40	1.45	1.50
0.05	0.3	4.5	25.5	64.1	91.4	>99	>99	>99	>99
0.10	2.6	30.4	81.4	98.8	>99	>99	>99	>99	>99
0.15	8.1	61.4	97.4	>99	>99	>99	>99	>99	>99
0.20	16.1	81.1	>99	>99	>99	>99	>99	>99	>99
0.25	24.7	90.7	>99	>99	>99	>99	>99	>99	>99
0.30	32.4	95.1	>99	>99	>99	>99	>99	>99	>99
0.35	38.5	97.0	>99	>99	>99	>99	>99	>99	>99
0.40	42.7	97.9	>99	>99	>99	>99	>99	>99	>99
0.45	44.9	98.2	>99	>99	>99	>99	>99	>99	>99
0.50	45.1	98.2	>99	>99	>99	>99	>99	>99	>99

b)

Odds Ratio

MAF	1.10	1.15	1.20	1.25	1.30	1.35	1.40	1.45	1.50
0.05	0.3	7.5	44.4	87.2	>99	>99	>99	>99	>99
0.10	4.0	51.7	96.5	>99	>99	>99	>99	>99	>99
0.15	14.4	85.4	>99	>99	>99	>99	>99	>99	>99
0.20	29.0	96.4	>99	>99	>99	>99	>99	>99	>99
0.25	43.3	>99	>99	>99	>99	>99	>99	>99	>99
0.30	54.7	>99	>99	>99	>99	>99	>99	>99	>99
0.35	62.7	>99	>99	>99	>99	>99	>99	>99	>99
0.40	67.7	>99	>99	>99	>99	>99	>99	>99	>99
0.45	70.2	>99	>99	>99	>99	>99	>99	>99	>99
0.50	70.5	>99	>99	>99	>99	>99	>99	>99	>99

Supplementary Table 5

Risk allele frequencies for the eight sentinel SNP markers showing genome-wide significant association with PACG susceptibility. NP denotes 'non-polymorphic'.

	Risk allele frequencies for each SNP							
	EPDR1 **rs3816415**	***GLIS3*** **rs736893**	***DPM2-FAM102A*** **rs3739821**	***CHAT*** **rs1258267**	***FERMT2*** **rs7494379**	***COL11A1*** **rs3753841**	***PCMTD1-ST18*** **rs1015213**	***PLEKHA7*** **rs11024102**
Singapore GWAS1	0.108	0.742	0.269	0.745	0.557	0.317	0.0096	0.359
Singapore GWAS2	0.111	0.724	0.276	0.736	0.588	0.31	0.013	0.379
Singapore replication	0.116	0.728	0.295	0.757	0.594	0.263	0.017	0.376
Hong Kong GWAS1	0.133	0.732	0.275	0.787	0.59	0.335	0.014	0.342
Hong Kong replication	0.105	0.703	0.282	0.764	0.598	0.304	0.019	0.363
China GWAS2	0.105	0.713	0.279	0.758	0.64	0.304	0.019	0.41
China replication	0.104	0.685	0.263	0.743	0.65	0.288	0.021	0.427
Japan GWAS2	0.061	0.762	0.159	0.667	0.729	0.317	0.0016	0.436
Okinawa	0.053	0.812	0.128	0.579	0.737	0.304	0.0094	0.433
Korea GWAS2	0.078	0.718	0.197	0.724	0.707	0.308	0.016	0.46
Indonesia GWAS2	0.142	0.728	0.271	0.836	0.503	0.276	0.028	0.355
Malays GWAS1 &2	0.129	0.732	0.29	0.856	0.536	0.305	0.049	0.36
Vietnam GWAS1 &2	0.132	0.782	0.298	0.764	0.596	0.304	0.01	0.341
Vietnam replication	0.135	0.75	0.301	0.791	0.589	0.318	0.0076	0.37
Myanmar GWAS2	0.095	0.734	0.283	0.748	0.664	0.287	0.066	0.43
Philippines GWAS2	0.158	0.707	0.259	0.785	0.517	0.345	0.034	0.31
Thailand GWAS2	0.133	0.774	0.287	0.8	0.596	0.364	0.037	0.346
South Indian GWAS1	0.133	0.723	0.455	0.943	0.626	0.442	0.125	0.308
South Indian replication	0.151	0.761	0.44	0.94	0.628	0.428	0.114	0.315
North Indian replication	0.152	0.646	0.438	0.946	0.693	0.469	0.122	0.393
Pakistan	0.137	0.727	0.474	0.956	0.67	0.38	0.096	0.308
Nepal	0.146	0.683	0.461	0.798	0.629	0.337	0.082	0.461
Saudi Arabia	0.127	0.824	0.537	0.988	0.694	0.475	0.114	0.071
Australia	0.113	0.657	0.765	NP	0.674	0.377	0.09	0.286
Poland	0.091	0.7	0.736	0.985	0.673	0.397	0.088	0.218
United Kingdom GWAS2	0.11	0.653	0.772	NP	0.69	0.386	0.089	0.293
Italy	0.182	0.691	0.739	NP	0.648	0.419	0.089	0.224
Mexico	0.136	0.863	0.667	0.975	0.848	0.221	0.034	0.406
United States	0.118	0.678	0.76	NP	0.671	0.379	0.076	0.265
Brazil GWAS2	0.111	0.734	0.633	0.956	0.717	0.478	0.119	0.172
Peru GWAS2	0.049	0.793	0.671	0.97	0.866	0.177	0.018	0.377

Supplementary Table 6

Association results for loci previously reported in primary open angle glaucoma (POAG).

					Association for POAG		Association for PACG		
CHR	**BP**	**SNP**	**Gene**	**A1/A2**	***P*-value**	**OR**	***P*-value**	**OR**	**Referemce**
1	165687205	rs4656461	*TMCO1*	A/G	0.66	6×10^{-14}	0.33	0.92	Burdon et al., 2011
1	165736880	rs7518099	*TMCO1*	A/G	0.67	4×10^{-13}	0.44	0.94	Burdon et al 2011
4	7853160	rs4619890	*AFAP1*	A/G	0.83	7.03×10^{-10}	0.28	0.96	Gharahkhani et al. 2014
4	7902003	rs4478172	*AFAP1*	A/C	0.84	2.19×10^{-8}	0.077	0.94	Gharahkhani et al. 2014
6	1922907	rs11969985	*GSMD*	A/G	0.76	7.70×10^{-10}	0.16	0.89	Gharahkhani et al. 2014
9	22068652	rs4977756	*CDKN2BAS*	A/G	1.39	1.4×10^{-14}	0.23	1.03	Burdon et al., 2011
9	107695848	rs2472493	*ABCA1*	A/G	0.76	2.16×10^{-19}	0.07	0.89	Gharahkhani et al. 2014
9	107707353	rs2164560	*ABCA1*	A/G	1.37	1.06×10^{-10}	0.14	1.07	Chen et al., 2014
9	107710562	rs2472459	*ABCA1*	A/G	0.71	5.17×10^{-13}	0.14	0.91	Chen et al., 2014
11	**120346360**	**rs2276035**	***ARHGEF12***	**A/G**	**1.18**	**7.83×10^{-6}**	**0.00024**	**1.11**	**Gharahkhani et al. 2014**
16	8896931	rs3785176	*PMM2*	A/C	0.77	6.05×10^{-7}	0.38	1.02	Chen et al., 2014
17	**10031090**	**rs12150284***	***GAS7***	**A/G**	**0.8**	**2.98×10^{-13}**	**0.00065**	**0.92**	**Hysi et al., 2014**

*r2 with index reported SNP rs9913911: 0.76 in Japanese, 0.961 in Han Chinese, 1.00 in Caucasians, 0.89 in Italians, and 0.88 in Africans.

A1/A2: Effect allele / other allele

SNPs showing evidence of association surpassing Bonforroni correction for 12 tests ($P<0.004$) are denoted in **bold**.

Supplementary Table 7

Association results for the 8 genome-wide significant PACG SNPs in Singaporean Chinese patients with primary open angle glaucoma (POAG; N = 968) and controls (N = 3,916)

CHR	SNP	BP	Effect Allele	Effect allele frequency	*P*-value for POAG susceptibility	OR for POAG susceptibility
1	rs3753841	103379918	G	0.31	0.036	1.12
7	rs3816415	37988311	A	0.11	0.017	1.20
8	rs1015213	52887541	A	0.015	0.81	1.05
9	rs736893	4217028	G	0.72	0.88	0.99
9	rs3739821	130702477	G	0.28	0.89	0.99
10	rs1258267	50895770	A	0.74	0.10	1.10
11	rs11024102	17008605	G	0.39	0.81	1.01
14	rs7494379	53411391	G	0.60	0.0022	0.85

Supplementary Table 8

Association results for loci previously reported to show genome-wide significant association with ocular axial length.

					PACG analysis		Axial length meta-analysis[a]			
SNP	CHR	BP	Effect Allele	Other Allele	ORmeta	Pmeta	EAF	Effect	StdErr	P.value
rs11264067	1	37764045	T	C	1.01	0.68	0.5382	0.0611	0.01	1.15E-09
rs4653300	1	37796641	T	C	0.99	0.70	0.4017	-0.056	0.0102	4.30E-08
rs10908355	1	37807873	T	G	1.01	0.74	0.588	0.0553	0.01	3.02E-08
rs4415526	1	37844315	T	C	1.09	0.17	0.4098	-0.055	0.0102	6.82E-08
rs4652964	1	37850887	A	G	0.99	0.84	0.4579	-0.063	0.0101	5.16E-10
rs12144790	1	37861701	T	C	0.94	0.060	0.288	0.0793	0.0124	1.81E-10
rs4074961	1	37865310	T	C	0.95	0.025	0.4361	0.0728	0.01	3.97E-13
rs1652333	1	205537083	A	G	1.05	0.052	0.5914	-0.056	0.0105	8.49E-08
rs891376	1	205558112	T	C	0.96	0.27	0.4092	0.0562	0.0105	9.35E-08
rs11118343	1	217806530	T	G	1.07	0.056	0.54	-0.067	0.0103	8.43E-11
rs4428898	1	217806589	A	G	0.97	0.25	0.5204	0.0625	0.01	4.32E-10
rs4373767	1	217826305	T	C	0.96	0.10	0.4634	0.0688	0.0102	1.66E-11
rs11118356	1	217843733	T	C	0.87	0.033	0.574	0.0691	0.0102	1.12E-11
rs10779363	1	217853513	T	C	0.94	0.035	0.5114	0.0662	0.0101	5.13E-11
rs7544369	1	217856085	T	C	0.99	0.83	0.4886	-0.066	0.0101	5.93E-11
rs793439	3	101120473	A	G	0.91	0.12	0.4588	0.0644	0.012	7.35E-08
rs12488245	3	101317944	T	C	1.03	0.46	0.5809	-0.057	0.0101	1.68E-08
rs9811920	3	101326983	A	G	0.99	0.74	0.3975	0.0803	0.0122	4.85E-11
rs6767441	3	101345873	T	C	1.01	0.71	0.5809	-0.057	0.0101	1.22E-08
rs12193446	6	129861731	A	G	NP	NP	0.9092	0.1219	0.0214	1.24E-08
rs11073058	15	32776918	T	G	0.97	0.42	0.4532	0.0661	0.01	4.34E-11
rs580839	15	32786121	A	G	0.96	0.51	0.456	0.0634	0.01	1.89E-10
rs560766	15	32788234	A	G	0.96	0.48	0.4563	0.0623	0.0099	3.66E-10
rs634990	15	32793365	T	C	1.01	0.73	0.5059	-0.065	0.0101	1.50E-10
rs683922	15	32795968	T	C	1.02	0.66	0.5508	-0.059	0.01	5.50E-09
rs669487	15	32797167	T	C	1.01	0.67	0.5539	-0.056	0.0102	4.29E-08
rs7495602	15	34375288	A	G	1.02	0.58	0.0863	0.1244	0.0228	5.15E-08
rs2179129*	22	27783193	A	G	1.02	0.53	0.4585	-0.055	0.01	4.08E-08

a Cheng CY et al., ***Am J Hum Genet 2013***; 93:264-277 *r^2 = 0.99 with the index previously reported SNP rs12321

NP: non-polymorphic

Supplementary Table 9

Supplementary Table 10

Expression quantitative trait locus (eQTL) output for rs3739821 on chromosome 9 and rs7494379 on chromosome 14. The output is obtained from the Genotype-Tissue Expression (GTEx) project (http://www.gtexportal.org/home/)[17].

Gencode Id	Gene Symbol	SNP Id	P-Value	Effect Size	Tissue
ENSG00000167103.7	*PIP5KL1*	rs3739821	9.20E-13	-0.52	Artery - Tibial
ENSG00000167103.7	*PIP5KL1*	rs3739821	3.60E-12	-0.63	Esophagus - Muscularis
ENSG00000167103.7	*PIP5KL1*	rs3739821	4.50E-12	-0.57	Adipose - Subcutaneous
ENSG00000167103.7	*PIP5KL1*	rs3739821	3.10E-10	-0.56	Nerve - Tibial
ENSG00000167103.7	*PIP5KL1*	rs3739821	7.50E-08	-0.66	Colon - Sigmoid
ENSG00000167103.7	*PIP5KL1*	rs3739821	9.70E-08	-0.68	Artery - Coronary
ENSG00000167103.7	*PIP5KL1*	rs3739821	1.50E-07	-0.61	Esophagus - Gastroesophageal Junction
ENSG00000167103.7	*PIP5KL1*	rs3739821	2.50E-07	-0.52	Heart - Left Ventricle
ENSG00000167103.7	*PIP5KL1*	rs3739821	0.0000015	-0.47	Artery - Aorta
ENSG00000136908.13	*DPM2*	rs3739821	0.0000017	-0.25	Thyroid
ENSG00000136908.13	*DPM2*	rs3739821	0.0000018	-0.19	Cells - Transformed fibroblasts
ENSG00000167103.7	*PIP5KL1*	rs3739821	0.0000051	-0.3	Breast - Mammary Tissue
ENSG00000167103.7	*PIP5KL1*	rs3739821	0.000006	-0.38	Colon - Transverse
ENSG00000198252.7	*STYX*	rs7494379	2.70E-07	-0.22	Adipose - Subcutaneous
ENSG00000198252.7	*STYX*	rs7494379	0.0000093	-0.17	Cells - Transformed fibroblasts

Nucleotide sequences for primers used in expression analysis.

Primer	Sequence (5' to 3')	Annealing Temp	Size	NCBI Reference Sequence Accession number#
DPM2 forward	CCGTTAGCCTGATCATCTTC	60°C	218bp	NM_003863.3
DPM2 reverse	GGACCTTCACTGAGCCTTCT			
FAM102A forward	AACCTGTCCAGCCCTGAG	60°C	155bp	NM_001035254.2
FAM102A reverse	CTGCTGGTGGACGTGTTG			
PIP5KL1 forward	CACAGTCTGCGGGTGGAC	60	189bp	NM_001135219.1
PIP5KL1 reverse	GGTCTTGCCCTGAAAGTTGAG			NM_173492.1
GLIS3 forward	CAACAAGTGTACGTTTGAA	55	247bp	NM_152629
GLIS3 reverse	CACATGCTTTCTTAGGGAACT			
FERMT2 forward	CCATCAGAATGTAGCTCA	55	159bp	NM_006832
FERMT2 reverse	CGAATCAGTCTGTTGTATGCA			
EPDR1 forward	GATGTTTCAGATTGACCAAGCCA	58	210bp	NM_017549
EPDR1 reverse	CAATCCTTGACTGTATAGATGCC			
ACTB forward	CCAACCGCGAGAAGATGA	As amplification and normalizing control		
ACTB reverse	CCAGAGGCGTACAGGGATAG			

#These transcripts encoded the protein isoform with the "canonical" sequence according to UniProtKB (http://www.uniprot.org/uniprot/)

Supplementary References

1. Foster, P.J., Buhrmann, R., Quigley, H.A. & Johnson, G.J. The definition and classification of glaucoma in prevalence surveys. *Br J Ophthalmol* **86**, 238-42 (2002).
2. Ong, E.L. *et al.* The utility of symptoms in identification of primary angle-closure in a high-risk population. *Ophthalmology* **115**, 2024-9 (2008).
3. Bei, J.X. *et al.* A genome-wide association study of nasopharyngeal carcinoma identifies three new susceptibility loci. *Nat Genet* **42**, 599-603 (2010).
4. Dunstan, S.J. *et al.* Variation at HLA-DRB1 is associated with resistance to enteric fever. *Nat Genet* **46**, 1333-6 (2014).
5. Khor, C.C. *et al.* Genome-wide association study identifies susceptibility loci for dengue shock syndrome at MICB and PLCE1. *Nat Genet* **43**, 1139-41 (2011).
6. Vithana, E.N. *et al.* Genome-wide association analyses identify three new susceptibility loci for primary angle closure glaucoma. *Nat Genet* **44**, 1142-6 (2012).
7. Consortium, U.I.G. *et al.* Genome-wide association study of ulcerative colitis identifies three new susceptibility loci, including the HNF4A region. *Nat Genet* **41**, 1330-4 (2009).
8. Davila, S. *et al.* Genome-wide association study identifies variants in the CFH region associated with host susceptibility to meningococcal disease. *Nat Genet* **42**, 772-6 (2010).
9. Khor, C.C. *et al.* Genome-wide association study identifies FCGR2A as a susceptibility locus for Kawasaki disease. *Nat Genet* **43**, 1241-6 (2011).
10. International Stroke Genetics, C. *et al.* Genome-wide association study identifies a variant in HDAC9 associated with large vessel ischemic stroke. *Nat Genet* **44**, 328-33 (2012).
11. Evans, D.M. *et al.* Interaction between ERAP1 and HLA-B27 in ankylosing spondylitis implicates peptide handling in the mechanism for HLA-B27 in disease susceptibility. *Nat Genet* **43**, 761-7 (2011).
12. Aung, T. *et al.* A common variant mapping to CACNA1A is associated with susceptibility to exfoliation syndrome. *Nat Genet* **47**, 387-92 (2015).
13. Png, E. *et al.* A genome-wide association study of hepatitis B vaccine response in an Indonesian population reveals multiple independent risk variants in the HLA region. *Hum Mol Genet* **20**, 3893-8 (2011).
14. Sakuntabhai, A. *et al.* A variant in the CD209 promoter is associated with severity of dengue disease. *Nat Genet* **37**, 507-13 (2005).
15. Gharahkhani, P. *et al.* Common variants near ABCA1, AFAP1 and GMDS confer risk of primary open-angle glaucoma. *Nat Genet* **46**, 1120-5 (2014).
16. Burdon, K.P. *et al.* Genome-wide association study identifies susceptibility loci for open angle glaucoma at TMCO1 and CDKN2B-AS1. *Nat Genet* **43**, 574-8 (2011).
17. Consortium, G.T. The Genotype-Tissue Expression (GTEx) project. *Nat Genet* **45**, 580-5 (2013).